

Hydrogen line observations: From frugal to advanced

Part 4: Observation Results with Different Antennas

Wolfgang Herrmann and the Astropheiler "Hydrogen Team"

1. Introduction

Observing the emission of neutral hydrogen from our galaxy has become a very achievable target for amateurs. Low cost components have become readily available over the recent years which substantially facilitate the observation possibilities. There are quite a few options to approach this goal, varying in technical and financial effort. Achievable results will be different, but as will be demonstrated some basic observations are possible with a very frugal approach.

In this series of articles, we have so far covered various options for antennas, amplifiers, filters and backends which can be used for the observation of the hydrogen emission. It is now time in this fourth part to start doing actual observation and to compare results obtained.

2. Observations procedure to compare different antennas

The most important part of this project has been to compare what can be achieved with different antennas. The starting point for the comparison is a reference setup with a 3 m dish as the antenna, described in more detail below in section 3. This 3 m dish was then replaced with all other antennas leaving the rest of the receiving chain untouched.

The evaluation of each antenna was performed by doing a transit scan observation of the hydrogen emission of our Milky Way galaxy. This was accomplished by placing the antennas pointing straight up. As the earth rotates, different parts of the Milky Way come into the view of the antenna. Observations were done over a full sidereal day. For our location, this represents a sky scan at a declination of about 50.5° over the right ascension range from 0 to 24 hrs.

The corresponding sky scan track in galactic coordinates is shown in fig. 1 as a red curve overlaid over a plot of the hydrogen density in the Milky Way. This hydrogen map is based on the comprehensive HI survey by the HI4PI collaboration [1]. As can be seen from the plot, an antenna looking straight up from our location will point at the galactic plane twice during a sidereal day. This happens at around RA=4:19 and RA=21:25. This is where the strongest signal can be expected.

The observation consisted of continuously taking spectra with an integration time of 5 minutes. Processing and writing to file added a few seconds, so during a full day's scan about 285 spectra were recorded.

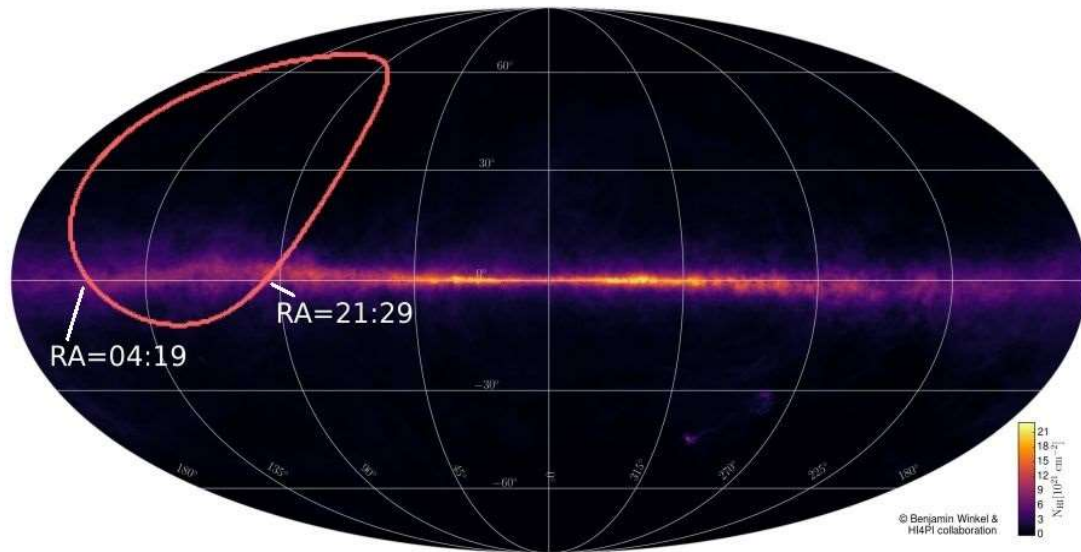


Figure 1: Scan Track in Galactic Coordinates overlaid with Hydrogen Density
 Source of Background Picture: Benjamin Winkel and the HI4PI Collaboration [1]

3. Reference setup

3.1. Hardware reference setup

In the previous articles of this series, 14 antennas, 12 types of amplifiers, 6 types of filters and 5 different SDRs have been described. Testing of each and every combination obviously is not possible.

Therefore, a “reference setup” has been defined and other selected setups have been tested against that reference setup.

The reference setup consisted of the following combination of the components described previously:

- The 3 m dish as described under section 7.14 of part one of this series of articles
- The Triquint TQP3M9037 low noise amplifier as described under section 3.2 of part two of this series as the first stage LNA
- The Radio Astronomy Supplies filter as described under section 4.6 of part two of this series
- The HackRF software defined radio as described under section 4.2 of part three of this series

In order to cover a lengthy cable run of about 30 m between the outdoor setup (LNA, filter) and the indoor electronics (HackRF), additional line amplifiers were added behind the filter to compensate the cable loss. The two Down East Microwave Amplifiers described under section 3.5 of part two of the series of articles have been used for that purpose.

The overall reference setup is shown in fig. 2.

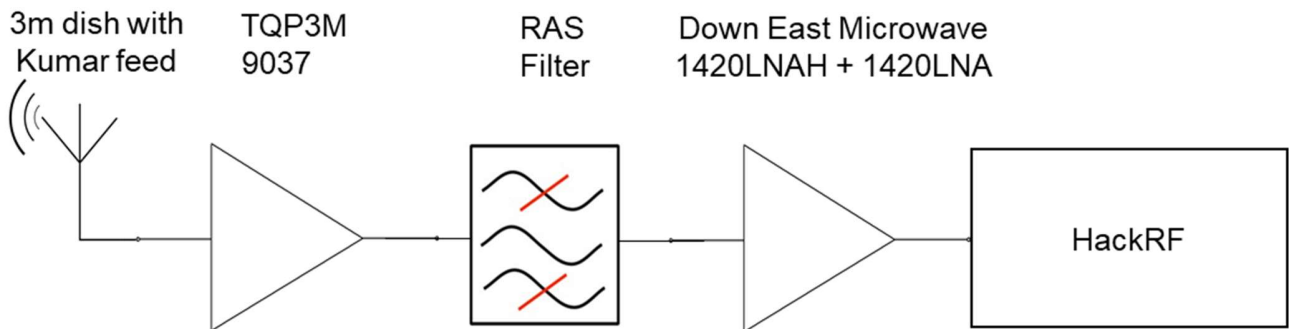


Figure 2: Reference Setup

3.2. Software

3.2.1. Spectrum capture

The software to capture hydrogen spectra with the HackRF was based on “soapy_power” [2]. This software is an application which uses “Soapy_SDR” [3] as an abstraction layer to communicate with the SDR.

The function of soapy_power is to set the desired parameters of the SDR, to capture the samples from the SDR and to perform a Fast Fourier Transform on the samples. The output is a power spectrum, i.e. the received power per frequency channel.

In our setup, soapy_power itself was embedded in a Python script which triggered the spectrum measurements with integration times of five minutes each and writing the results into a Flexible Image Transfer System (FITS) file [4]. The script also took care of providing metadata such as right ascension, declination, time and other relevant information for the header of the FITS file.

The settings for the SDR commanded by the script were 10 MHz sampling rate, 10 MHz filter width and maximum gain applicable to the HackRF. The setting for the Fourier Transform (FFT) was to provide 4096 spectral bins, resulting in a resolution of 2.441 kHz per spectral bin.

4. Evaluation procedure

4.1. Evaluation of individual spectra

Each transit scan with an antenna created a number of FITS files, each containing the spectrum obtained with 5 minutes integration time. As the sky moves through the antenna beam during a day, the spectra vary in intensity (reflecting the amount of hydrogen in the viewing angle) and peak position (due to the varying Doppler shift). From these various spectra, the one with the highest peak intensity was chosen. The sky location for this highest peak intensity was determined from the local sidereal time at the time of the recording of the spectrum, and the fixed declination of 50.5° as the antenna was pointing straight up. We called this sky location the “Best Spot” of the transit.

For the spectrum at the Best Spot, the signal to RMS noise ratio was determined as demonstrated in the example below.

The program CLASS from the GILDAS suite [5] was used for this purpose. This program is designed to process (among other applications) spectral observations. It allows baseline correction and to determine various parameters of a spectral observation.

An exemplary demonstration of this procedure is shown here.

First, the FITS file of interest is loaded into CLASS. From the total 10 MHz bandwidth only the part which contains the hydrogen line is of interest. Therefore, plotting and evaluation was restricted to the velocity range of -300 km/s to 300 km/s. This corresponds roughly to the frequency range 1419 to 1422 MHz. A typical spectrum is shown in fig. 3.

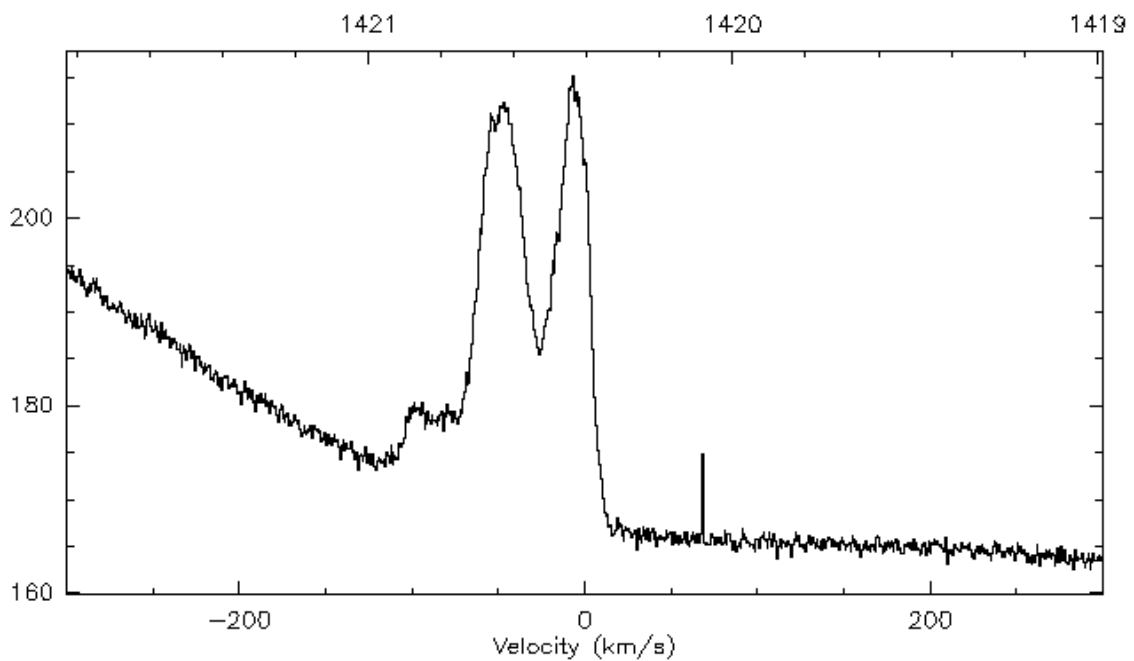


Figure 3: Spectrum as loaded from FITS file

The vertical axis is in arbitrary units, the horizontal axes are the frequency in MHz (top) and the corresponding velocity in km/sec (bottom)

Obviously, there is a baseline variation due to imperfections in the spectral response of the amplifiers, filters and the SDR. Also, in this case, there is a spurious narrow line from RFI. In order to eliminate the baseline, a polynomial is fitted to the baseline. The purpose of this baseline elimination is removing this as an instrumental artefact for better comparison of spectra and to allow the determination of the background noise. In order to restrict the fitting process to the background area, windows are defined which include the actual signal and the spurious line.

This setting is shown in fig. 4.

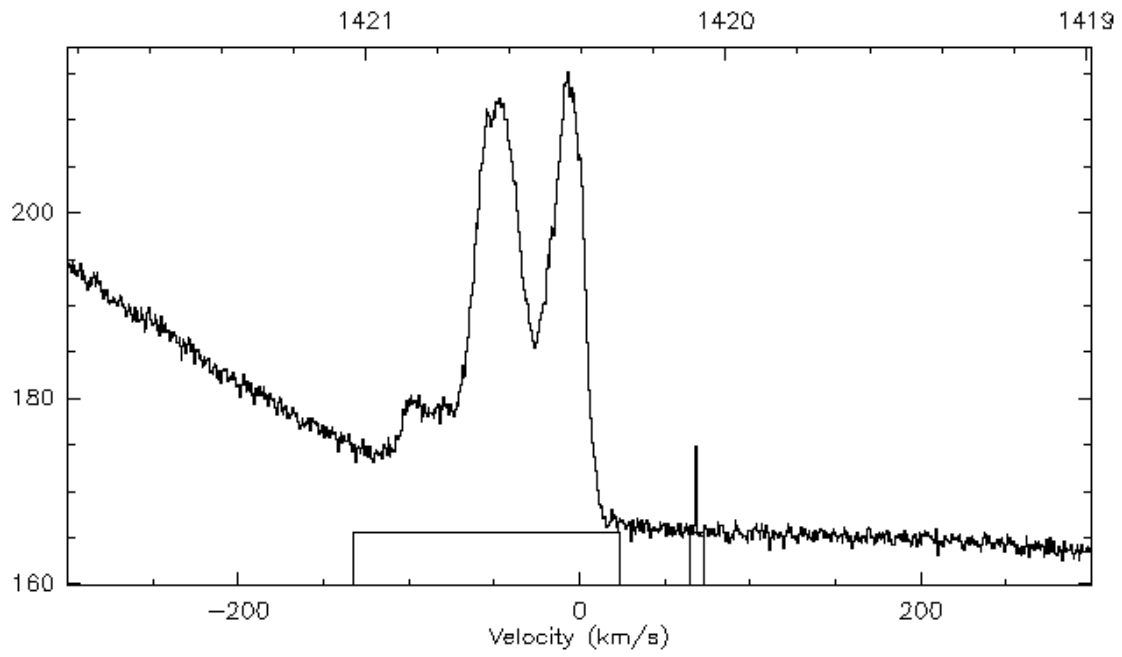


Figure 4: Spectrum with windows defined

Then the actual fit is done, the fitted curve is shown in fig. 5.

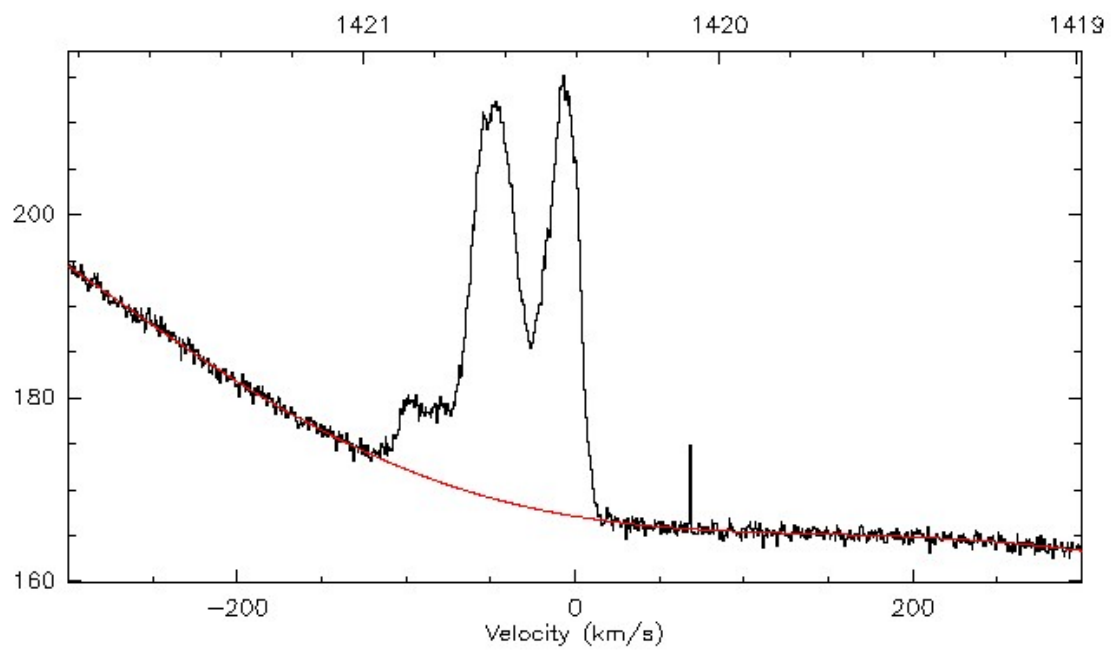


Figure 5: Spectrum with fitted curve

The fitted curve is then subtracted from the spectrum resulting in a flat baseline centred at 0 intensity as shown below in fig. 6.

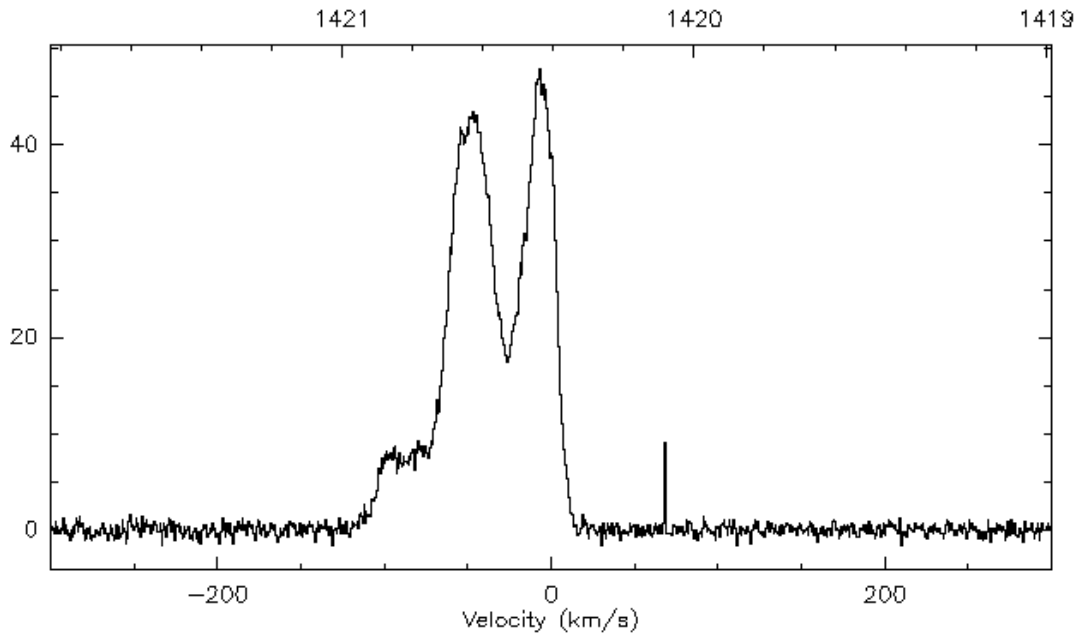


Figure 6: Baseline corrected spectrum

As part of the fitting process, CLASS also determines the rms fluctuation of the baseline which is provided in the fit result. In this case this has been 0.55. The peak can be determined from the graph to be 47.5. Therefore, in this example the signal to rms noise ratio is 86.3.

This procedure has been applied to each of the antenna measurements for the spectrum having the largest signal during the transit.

4.2. Generating heatmaps

In order to display the full transit with its many spectra, a heatmap has been generated as follows: There are about 285 spectra for each transit over a sidereal day. Each of these spectra has been baseline corrected with a procedure similar to what is explained above. However, due to the large number of spectra this process has been automated using a program written specifically for this purpose.

This resulted in about 285 baseline corrected spectra which were then combined into one graph. This graph shows the right ascension as the horizontal axis and the velocity of the hydrogen emission as the vertical axis. The intensity is displayed colour coded. Such a heatmap gives a qualitative impression of the spatial resolution.

A typical example of such a heatmap is shown below in fig. 7.

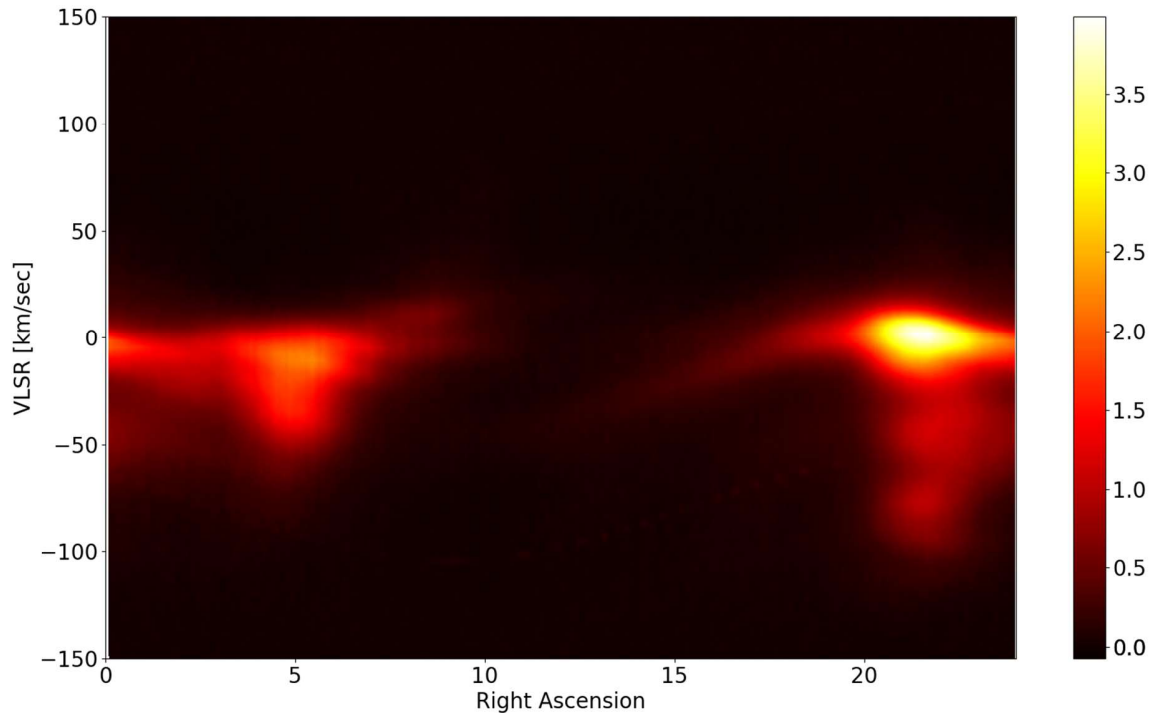


Figure 7: Example of a heatmap

4.3. Note on intensities

The intensity shown in both the single spectra and in the heatmaps denote received power, the scale is linear. All intensities are uncalibrated, so they are arbitrary units. A direct comparison between the intensities for different antennas as shown in section 5 should be taken with some caution. We found that over the time span of several months during which the measurements were taken, there were some fluctuations and changes of the overall gain of the receiving chain.

For a quantitative assessment of the quality of the signal from various antennas the SNR therefore is a better measure and comparison has been based on this quantity.

4.4. Note on correction for local standard of rest

When observing the emission of hydrogen, the actual frequency (and, hence, the velocity) observed is influenced by the motion of the observer itself. There is a Doppler shift introduced by the rotation of the earth, the rotation of the earth around the sun, the influence of the moon and some other minor factors. Therefore, the frequency will vary with the date and time of the observation. This is undesirable as it makes comparison of different observations from different observatories and observation times difficult.

Therefore, it is common practice to correct an observation to eliminate this effect. The procedure is to calculate the speed of the observatory in the direction of the observation with respect to the solar system barycentre. In addition, the convention is to assume a specific motion of the solar system barycentre with respect to the local stars in the neighbourhood. This reference frame is called the “Local Standard of Rest (LSR)”.

Typically, for spectral observations in radio astronomy this correction with respect to the LSR is applied and the measured velocities are given as “VLSR” (the velocity referenced to the LSR). However, when the beam width of an antenna becomes very large, the direction of observation becomes more or less undefined. Radiation coming from different directions are summed up and cannot be distinguished. Different observing directions, however, require different LSR corrections. Therefore, an LSR correction for small antennas with a wide beam becomes meaningless.

Consequently, the measurements shown in this article for the various antennas have only been corrected with respect to the LSR where the beam was reasonably narrow. This applies to the parabolic dishes of 3 m and 90 cm. The data from all other antennas is shown with uncorrected velocities.

5. Observation results for different antenna

5.1. 3 m Dish (Reference setup)

The observation performed with the 3 m dish clearly shows the transit of the galactic plane at the expected right ascensions (fig.8.). Also, quite some structure from the different parts of the milky way is resolved.

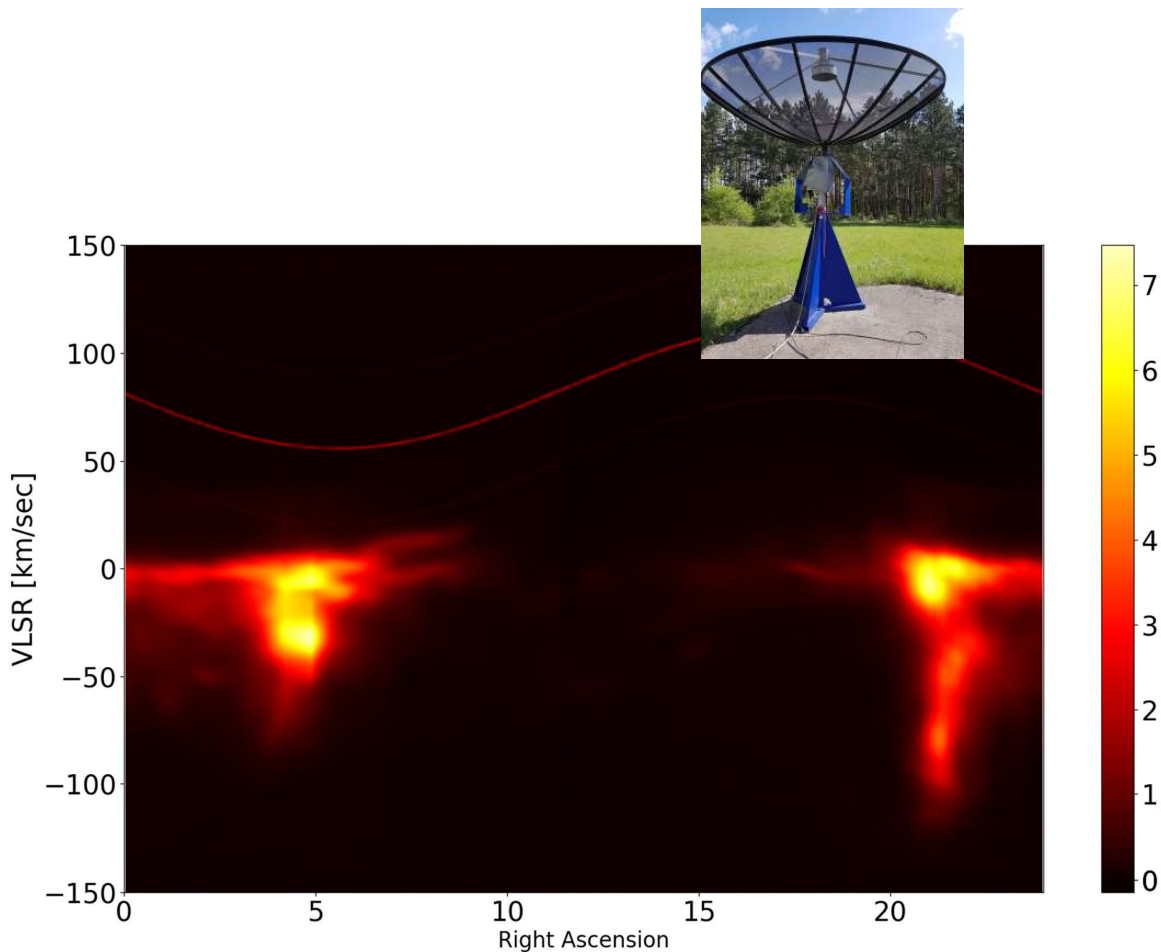


Figure 8: Transit scan with the 3 m dish

During this measurement, a spurious line (RFI) at a fixed frequency was encountered. Since this measurement was corrected for the local standard of rest as explained above, this is converted to a varying velocity. The sinusoidal behaviour is a direct consequence of the varying velocity towards the direction of observation due to the rotation of the earth.

The strongest signal was encountered at RA 4:34. The corresponding spectrum is shown below in fig. 9.

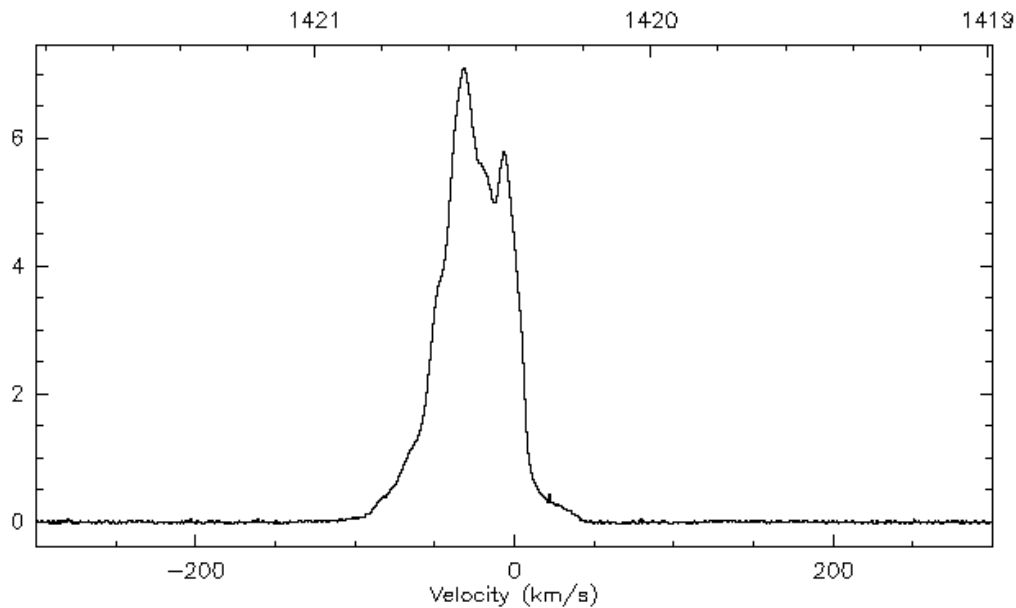


Figure 9: Spectrum with the 3 m dish at RA 4:34; SNR 528

The peak signal to rms noise of this spectrum is 528.

5.2. 90 cm Dish “Mini-Arecibo”

Results with the 90 cm dish are in principle similar to what can be observed with the 3 m dish. However, the larger beam width results in less spatial resolution. The structure is more “blurred” as shown in fig. 10.

In this case the transit of the galactic plane at RA 20:44 gives the maximum signal which has a peak signal to rms noise of 260. The spectrum is shown in fig. 10. It should be noted that even though the collecting area of this dish is only 9% of the 3 m dish, the signal to noise is still about half of what can be achieved with the 3 m dish. This nicely demonstrates how the loss of collecting area is partially compensated by the wider beam and hence, more hydrogen volume observed.

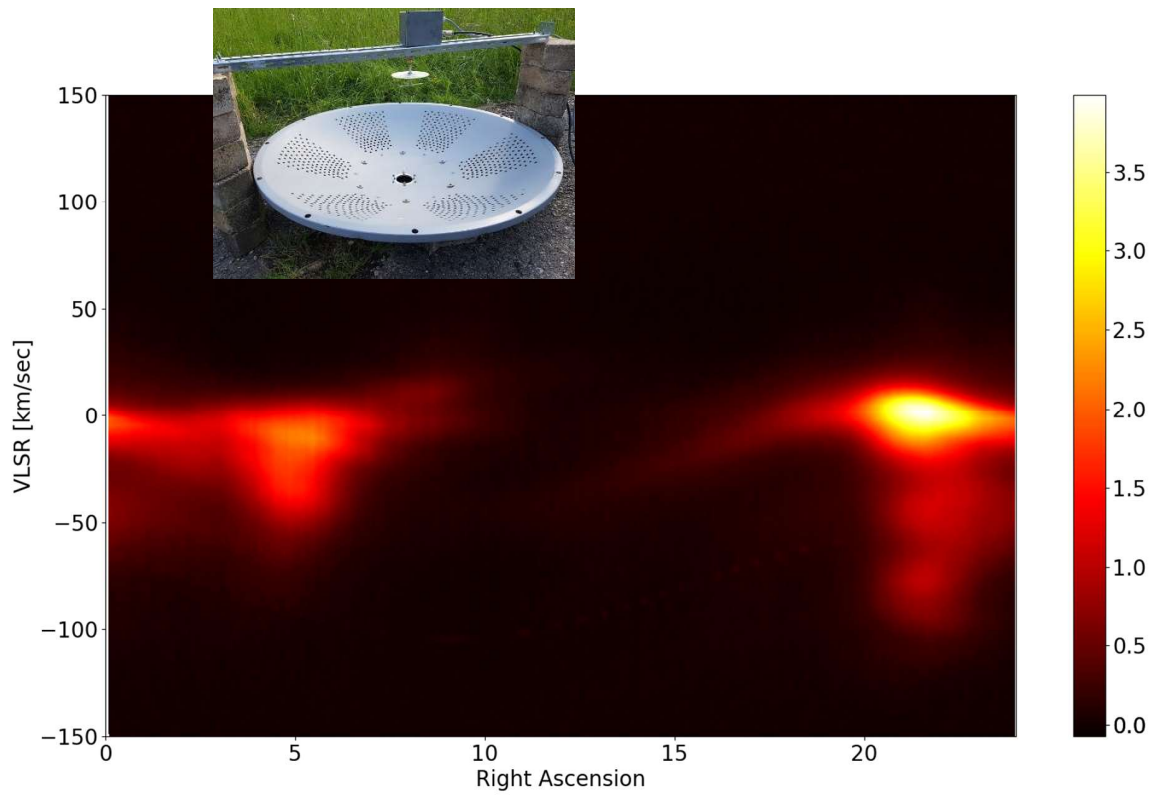


Figure 10: Transit scan with the 90 cm dish

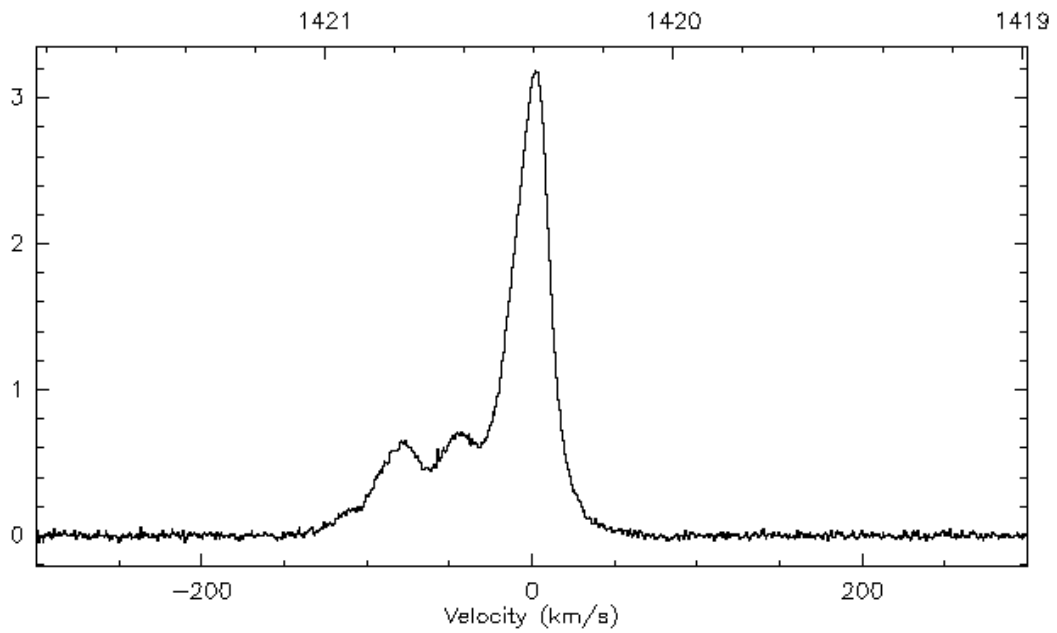


Figure 11: Spectrum with the 90 cm dish at RA 20:44; SNR 260

5.3. Corner Cube Antenna

Comparing the corner cube antenna with the 90 cm dish, there is a bit of a loss of spatial resolution as demonstrated by the transit scan shown in fig. 12.

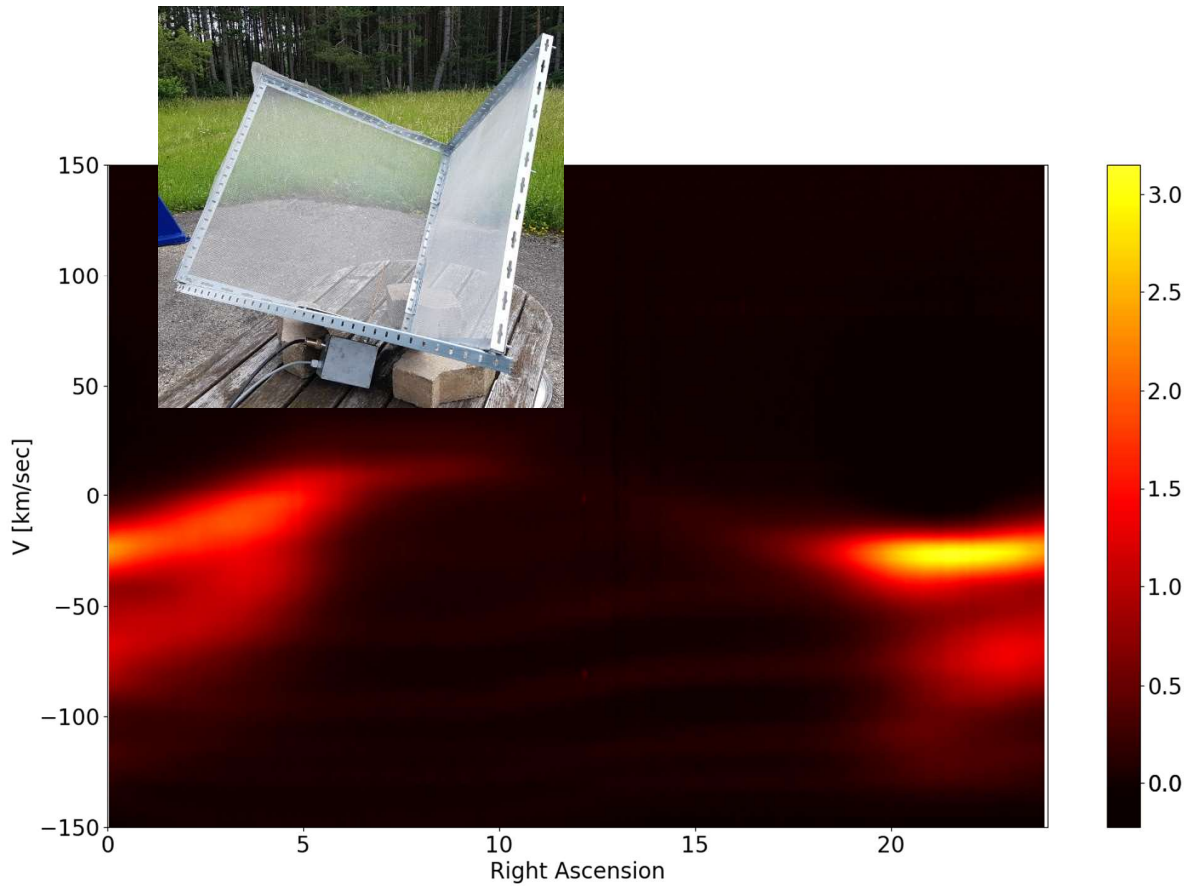


Figure 12: Transit scan with the corner cube antenna

The corner cube antenna comes in 3rd with respect to peak signal to rms noise ratio, which is 231. This is achieved at RA 21:30. This also differs slightly from where the maximum can be found with the 90 cm dish. This can be explained by a possibly different beam pattern. Also, the nominal orientation with the main beam looking straight up may have not been quite correct given the specific shape of this antenna.

The spectrum at maximum signal to rms noise is shown in fig 13. The measurement of this antenna has been impaired by RFI which can be clearly seen in the spectrum. Therefore, only the part > 0 km/s was used to evaluate the rms noise.

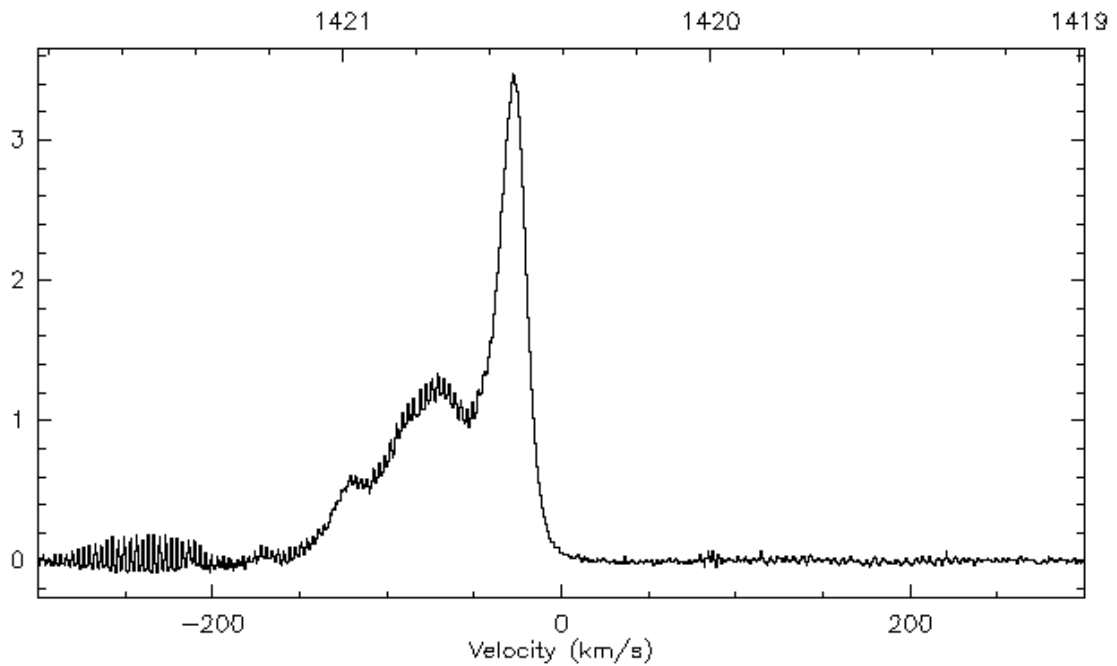


Figure 13: Spectrum with the corner cube antenna at RA 21:30; SNR 231 (impaired by RFI)

5.4. 60 cm Dish “Micro-Arecibo”

The 60 cm dish seems to be quite similar in performance to the corner cube antenna. Also, this measurement was impaired by RFI which created some artefacts in the heatmap from the transit scan, shown in fig. 14.

The RFI made it also difficult to determine the rms noise. In this case, there had to be some estimation which ended up at a peak signal to rms noise of 212. Due to the uncertainty in the assessment of the rms noise this figure has quite an error margin. It may very well be that this antenna actually performs somewhat better than the corner cube antenna.

The maximum signal was achieved at RA 19:54, the corresponding spectrum is shown in fig. 15.

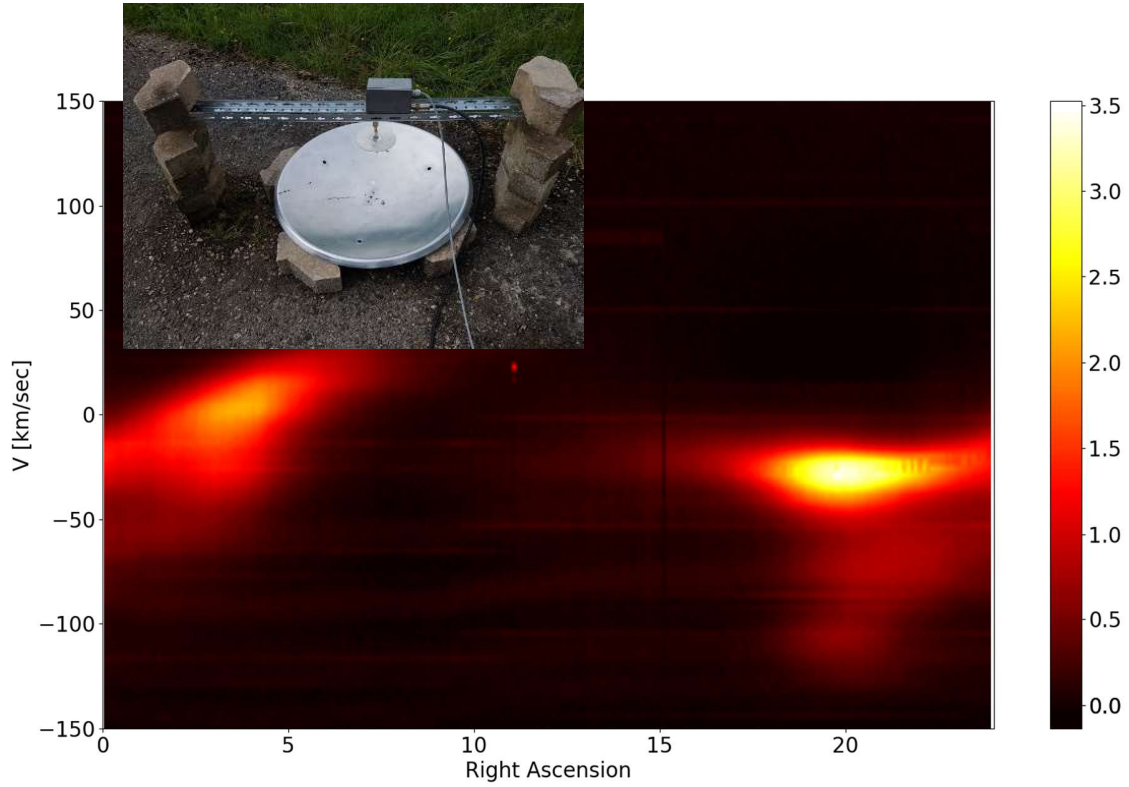


Figure 14: Transit scan with the 60 cm dish

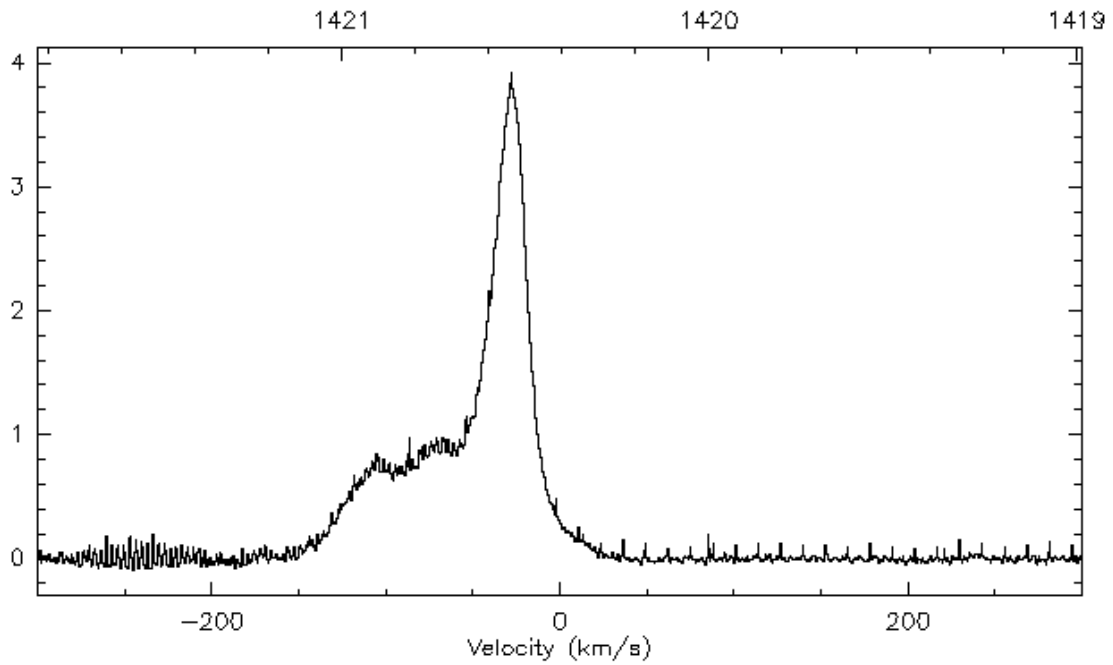


Figure 15: Spectrum with the 60 cm dish at RA 19:54; SNR 212

5.5. L-Band Horn

Unfortunately, also testing of the L-Band horn was impaired by RFI. In addition, during this measurement a jump in gain occurred for unknown reason. The results should therefore be interpreted with some caution. Nevertheless, it seems that such a horn is a relatively good antenna for hydrogen observations. Fig. 16 shows the outcome of the transit scan.

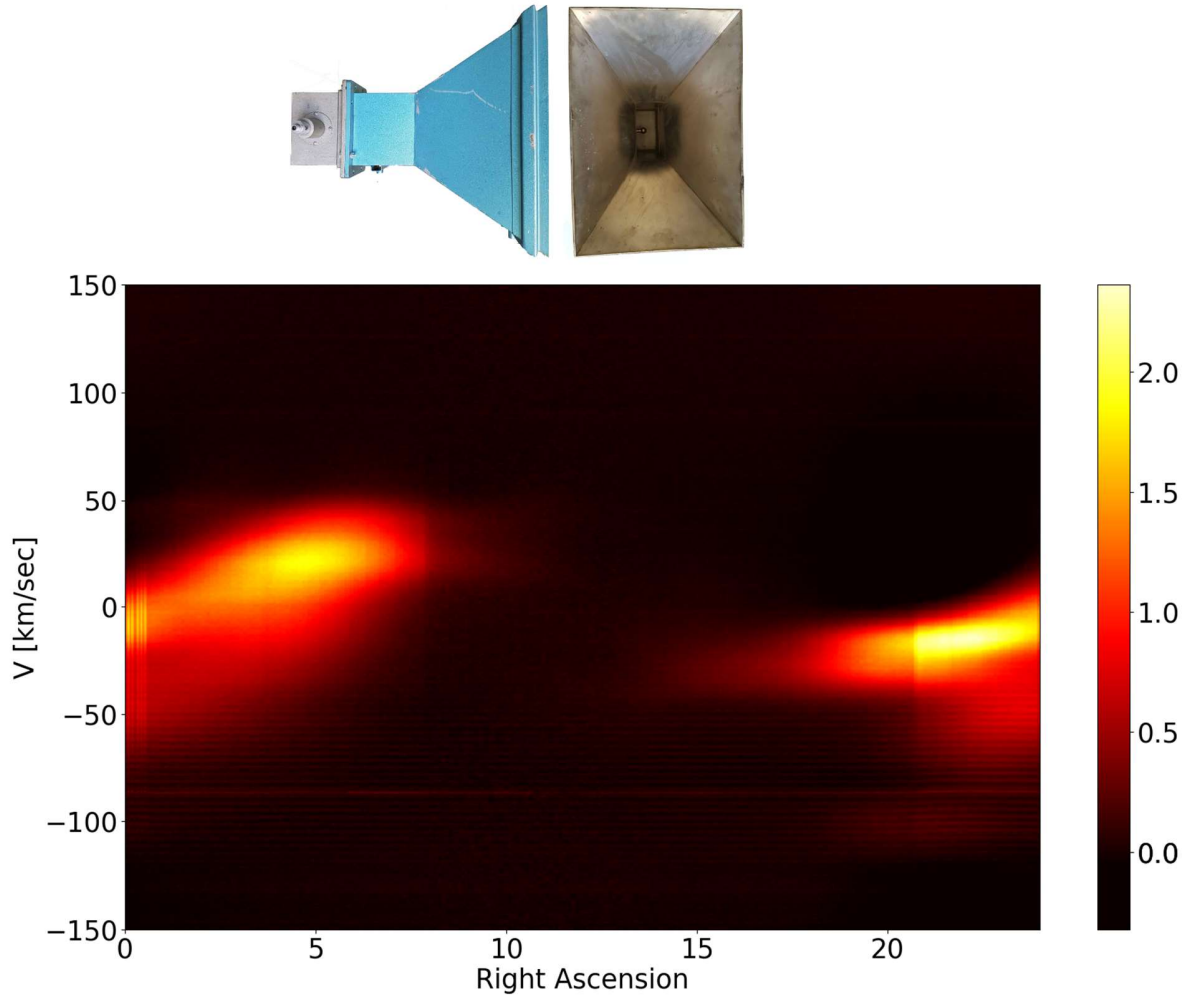


Figure 16: Transit scan with the L-Band Horn

The maximum signal was found at RA 22:06. There the peak signal to rms noise was 198. As in previous examples the part of the spectrum impaired by RFI was excluded from determining the rms noise.

The spectrum is shown in fig. 17.

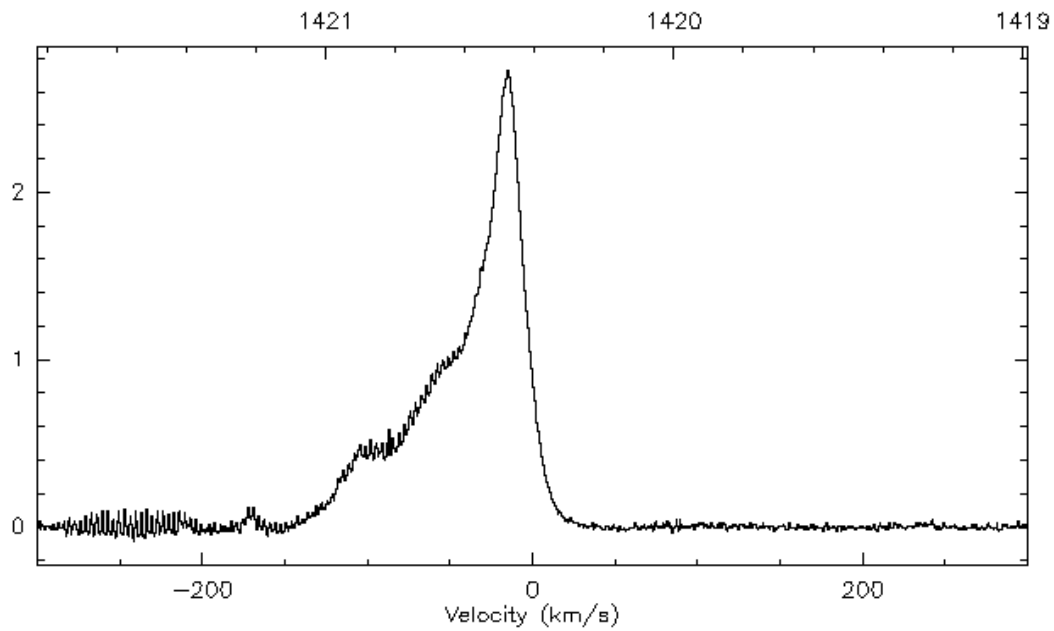


Figure 17: Spectrum with the L-Band Horn at RA 22:06; SNR 198

5.6. Patch Yagi

The Patch Yagi antenna is much smaller than the other antennas which were dealt with so far. Smaller antennas have a wider beam and therefore the heatmap from the transit scan shows less detail. This can be expected as the half power beam width is about 45° , so a lot of sky is covered at the same time. The transit scan is shown in fig. 18.

While the spatial resolution is less than with the bigger antennas, the achievable peak signal to noise ratio is still quite remarkable with 167. The maximum appears at RA 03:04

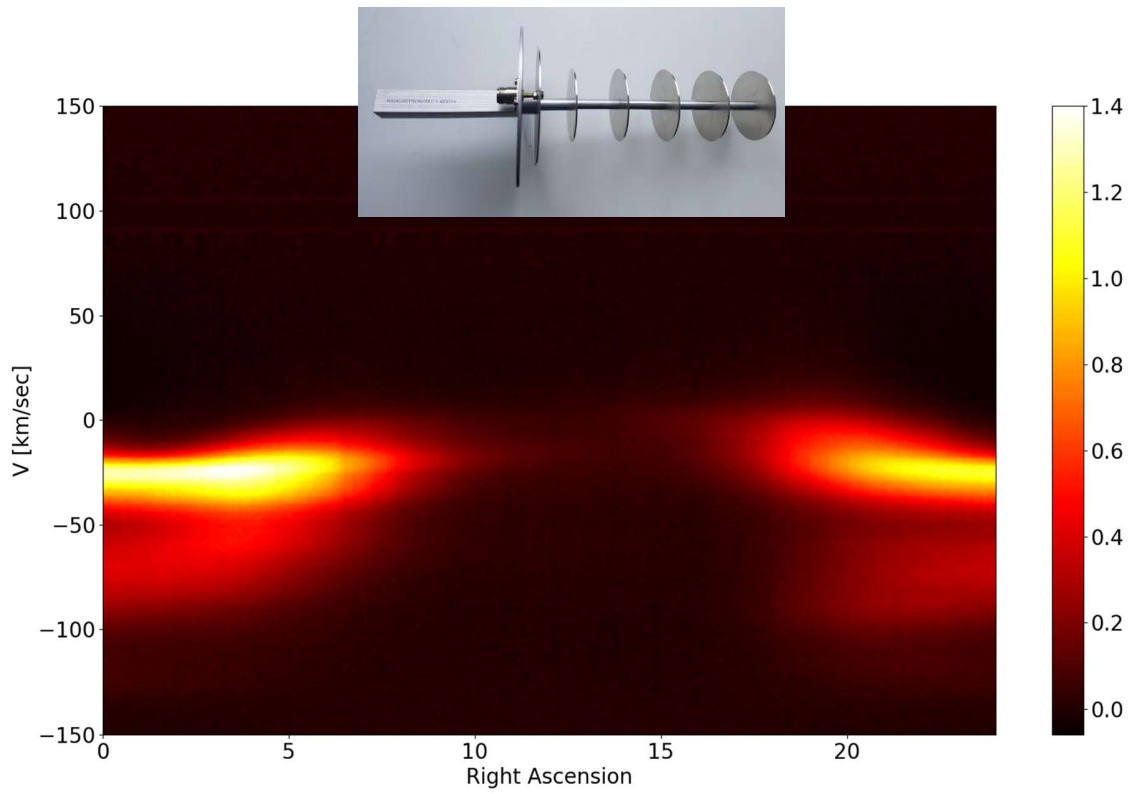


Figure 18: Transit scan with the Patch Yagi

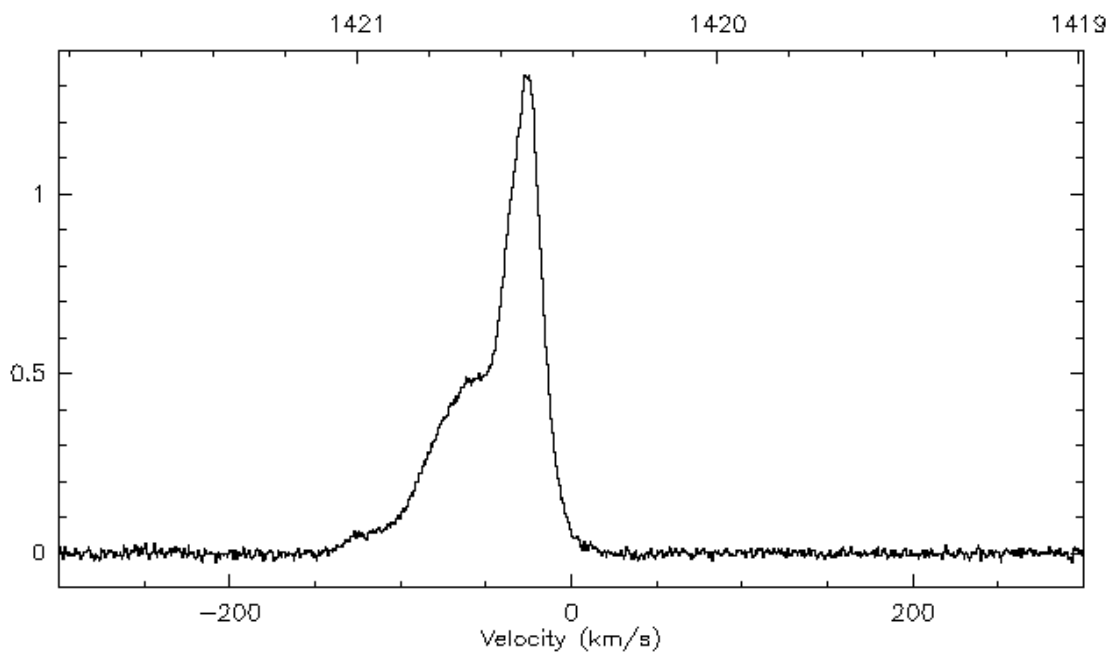


Figure 19: Spectrum with the Patch Yagi at RA 03:04; SNR 167

5.7. Circular waveguide “Stove Pipe”

The circular waveguide, which can very easily be built from a stove pipe is another nice example of a good signal received with a fairly small antenna. Given the small aperture and consequently wide beam the spatial resolution is limited as shown in fig. 20.

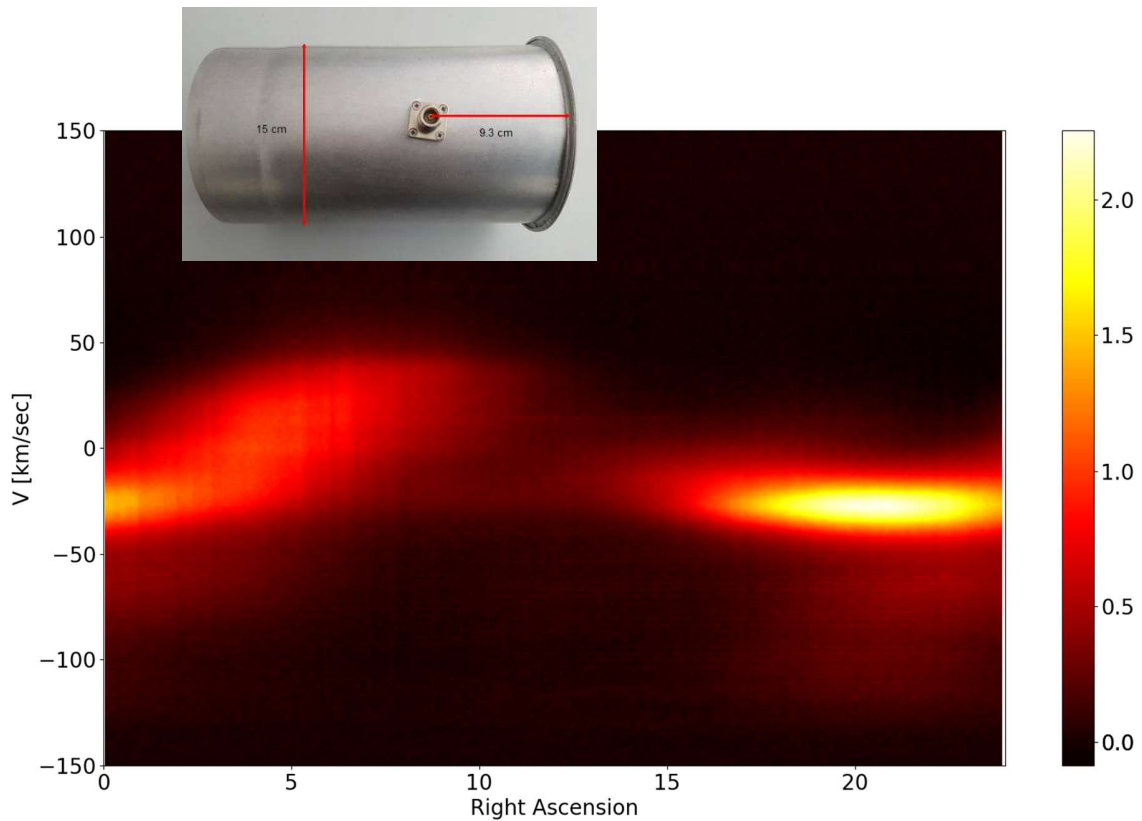


Figure 20: Transit scan with the circular waveguide “Stove Pipe” antenna

For this antenna the maximum is found at RA 19:36. Again some RFI is apparent in the spectrum which has been eliminated for the purpose of determining the SNR. Without this RFI the signal to rms noise ratio has been 135.

The spectrum is shown in fig. 21.

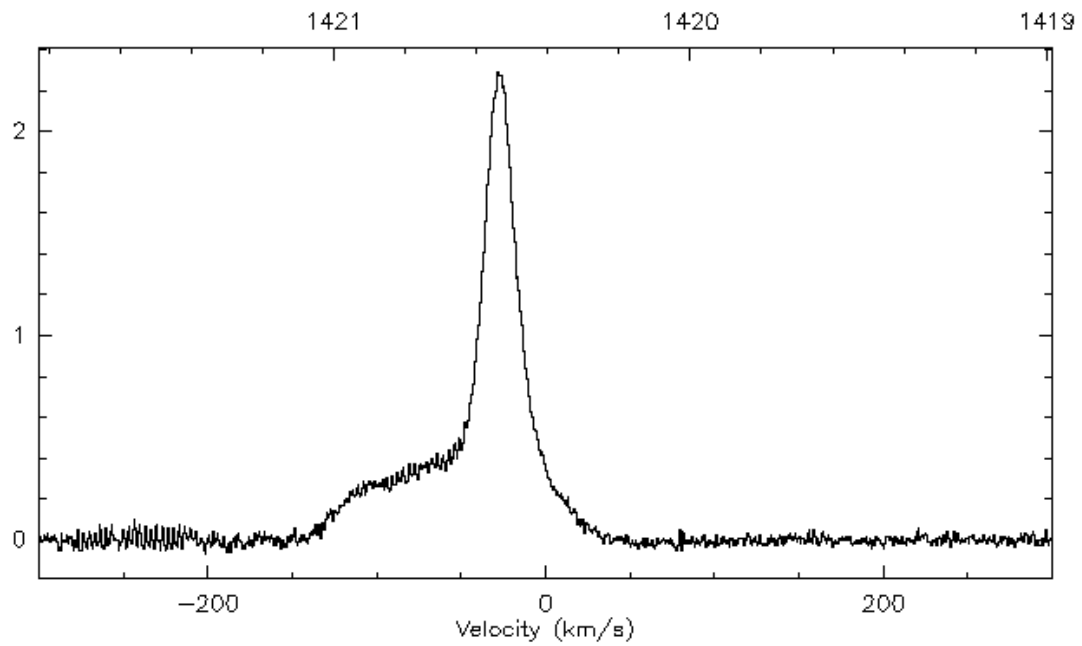


Figure 21: Spectrum with the “stove pipe antenna” at RA 19:36; SNR 135

5.8. Dipole with reflector

This simple antenna gives an amazingly good result. Built from semirigid cable and a CD, it provides a SNR quite similar to what has been achieved with the antenna shown before.

The transit scan is shown in fig 22.

The maximum signal was found at RA 19:38 with a SNR of 121 and the corresponding spectrum is shown in fig. 23.

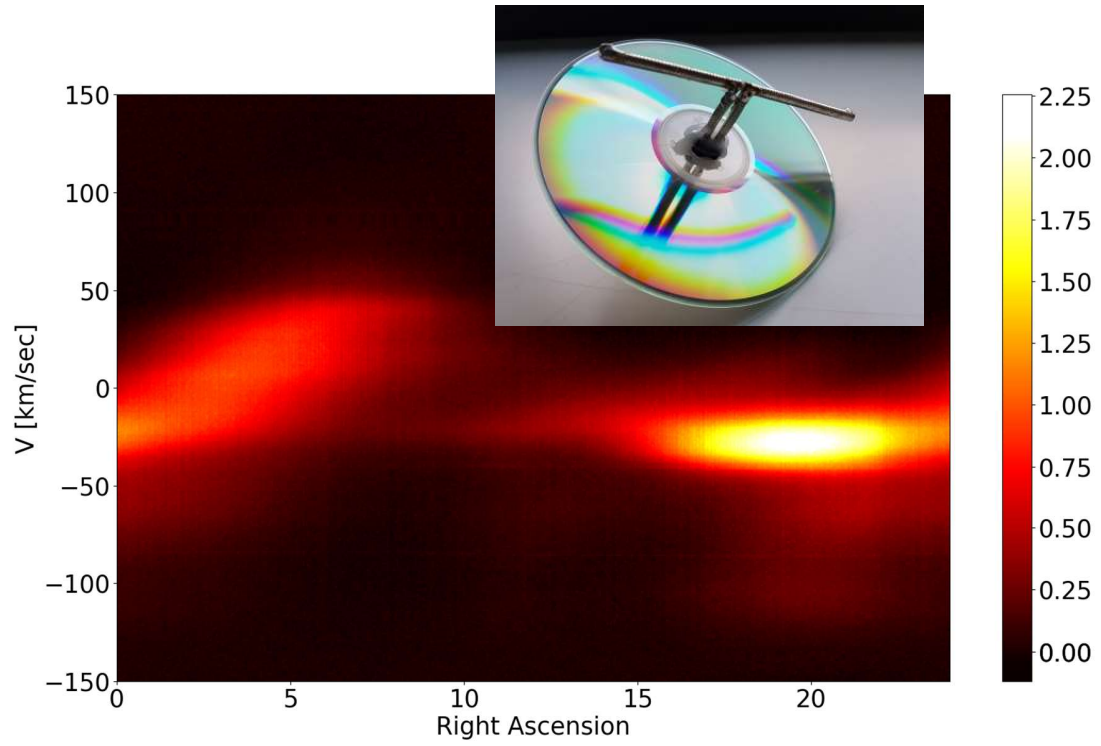


Figure 22: Transit scan with a dipole with reflector

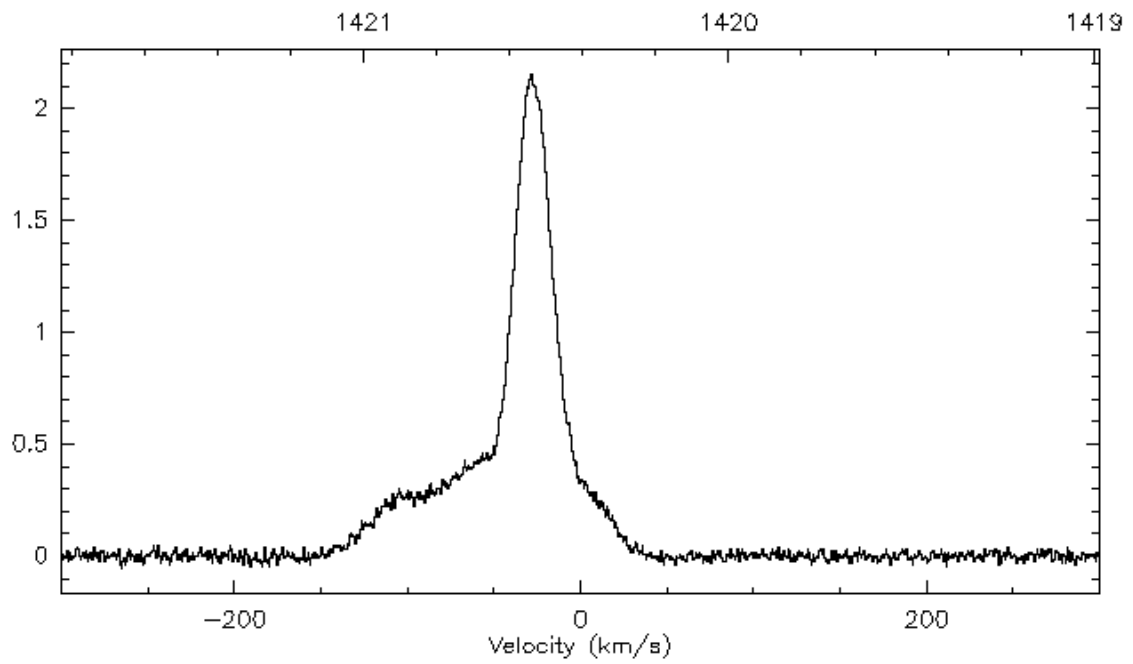


Figure 23: Spectrum with the Dipole/Reflector antenna at RA 19:38; SNR 121

5.9. L-Band rectangular waveguide

In this setup a L-band rectangular waveguide to coax adapter was used as an antenna. It is a similar device to the one attached to the horn as described in 5.5.

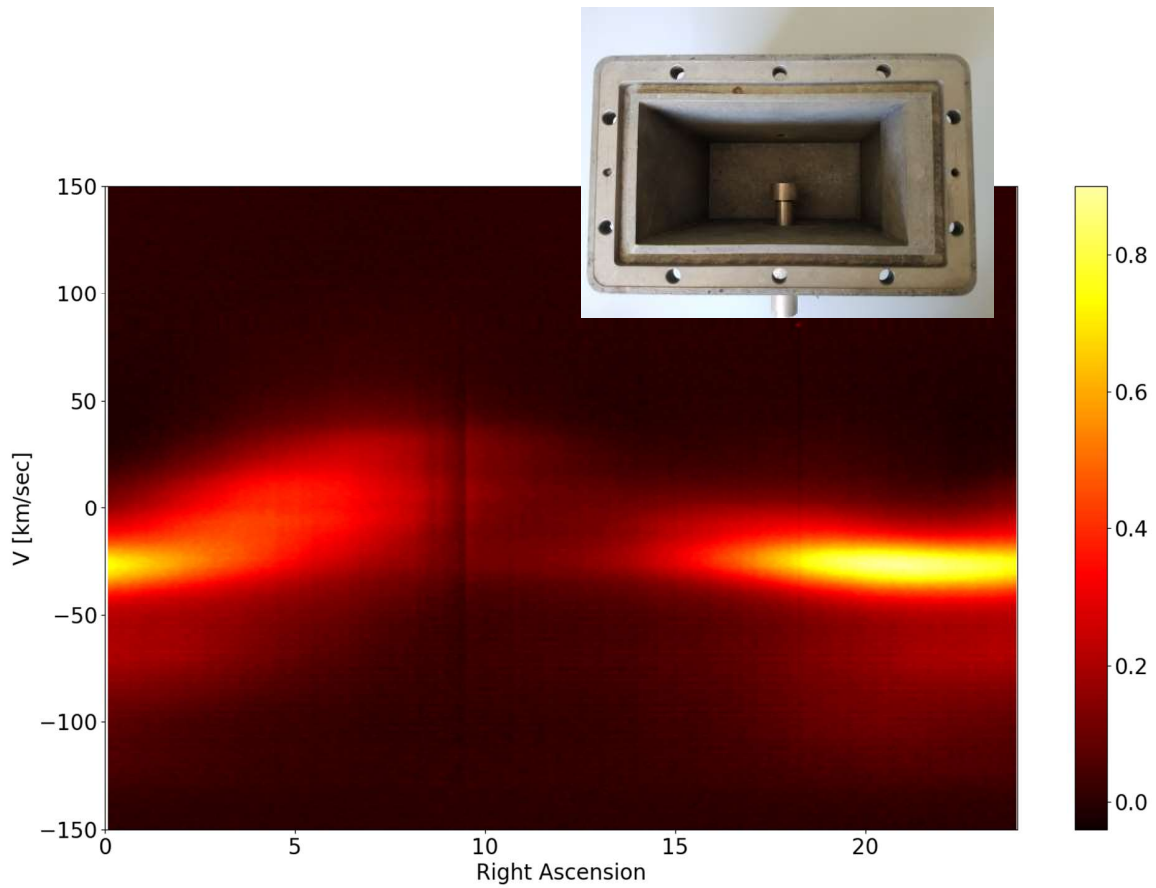


Figure 24: Transit scan with an L-band adapter as antenna

With this setup, the best signal to rms noise of 111 was achieved at RA 20:34. Fig. 24 shows the total transit. The corresponding spectrum is shown in fig. 25.

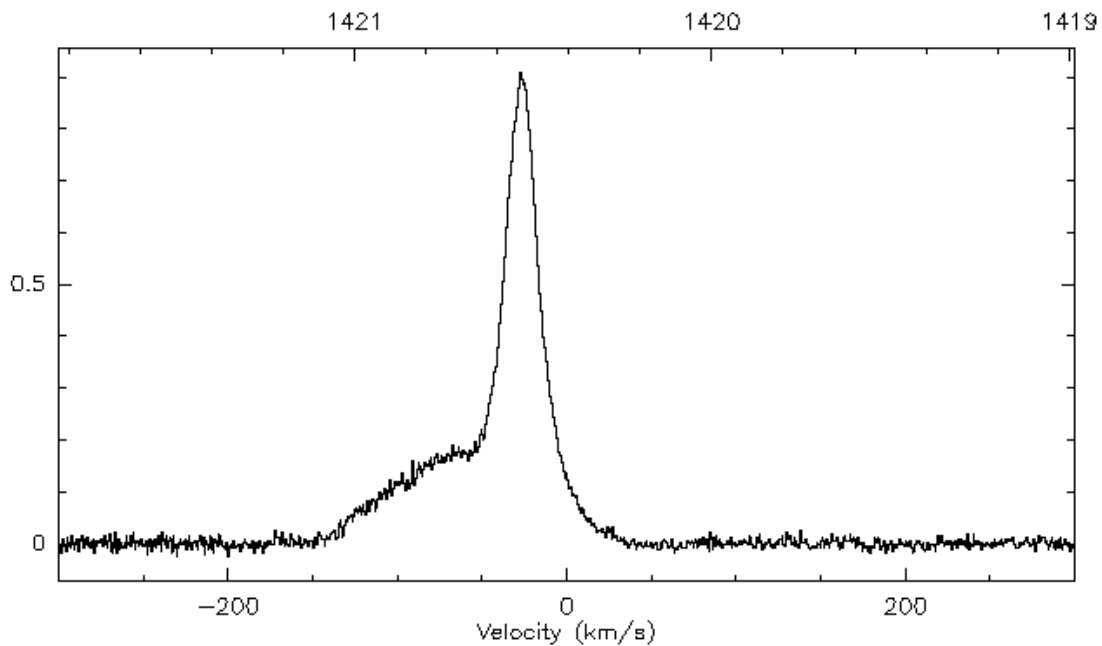


Figure 25: Spectrum with the L-band adapter at RA 20:34; SNR 111

5.10. Air gap patch antenna

The patch antenna is the next one demonstrating the reception of hydrogen emission. This is the only antenna from the ones investigated which is circularly polarized. Since the hydrogen emission is unpolarized, it is not expected to make any difference.

A SNR of 100 is quite remarkable for such a small device which measures only 165 mm across. The total transit is shown in fig 26.

The maximum SNR of 100 was seen at the RA of 20:10. The corresponding spectrum is shown below in fig. 27.

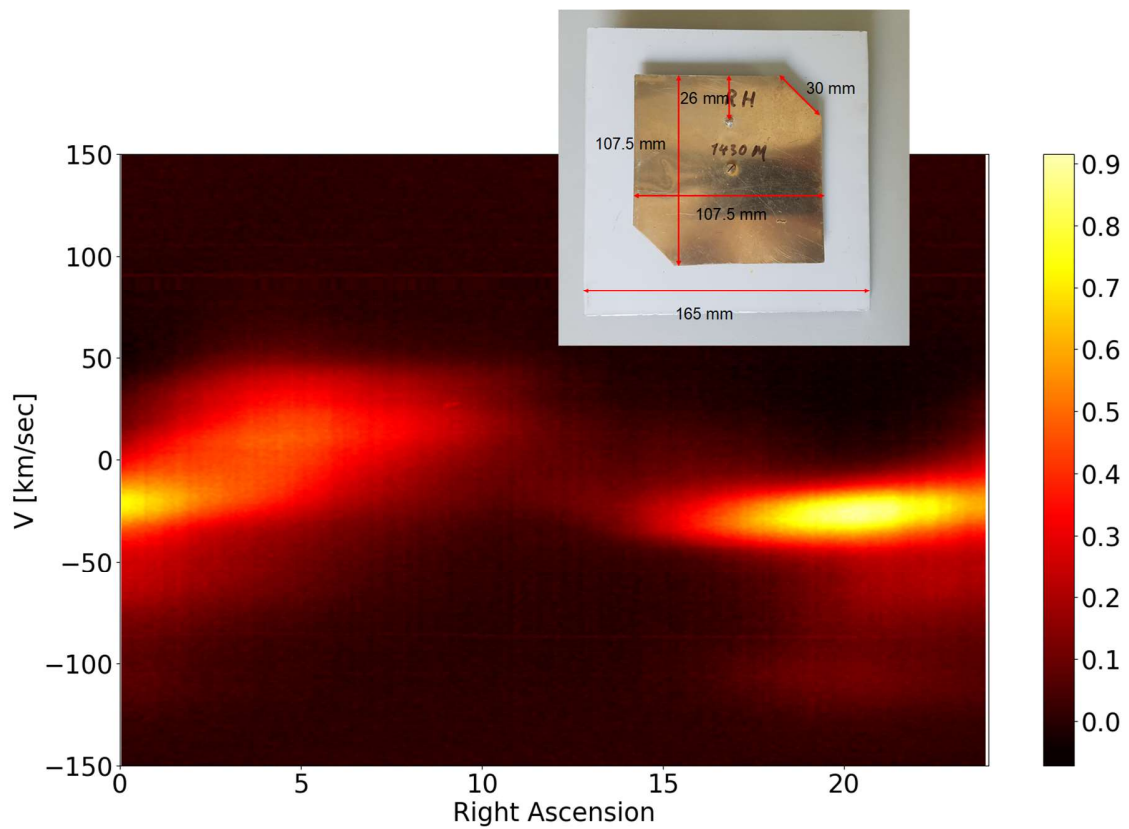


Figure 26: Transit scan with the air gap patch antenna

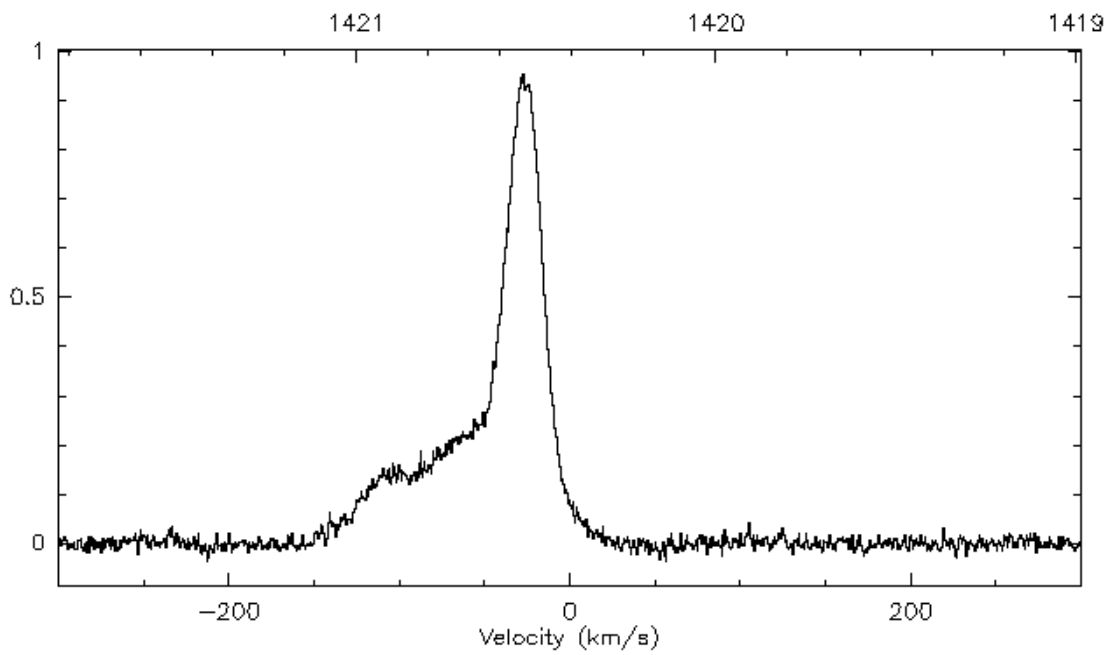


Figure 27: Spectrum with the Patch antenna at RA 20:10; SNR 100

5.11. Dipole with reflector, variant

This version of a dipole with reflector performs less well compared to the other variant described in 5.8. When the return loss measurements were done it was already apparent that there is a difference between the two versions [6]. Therefore, the lesser performance of this variant does not come as a surprise.

The transit is shown below in fig. 28.

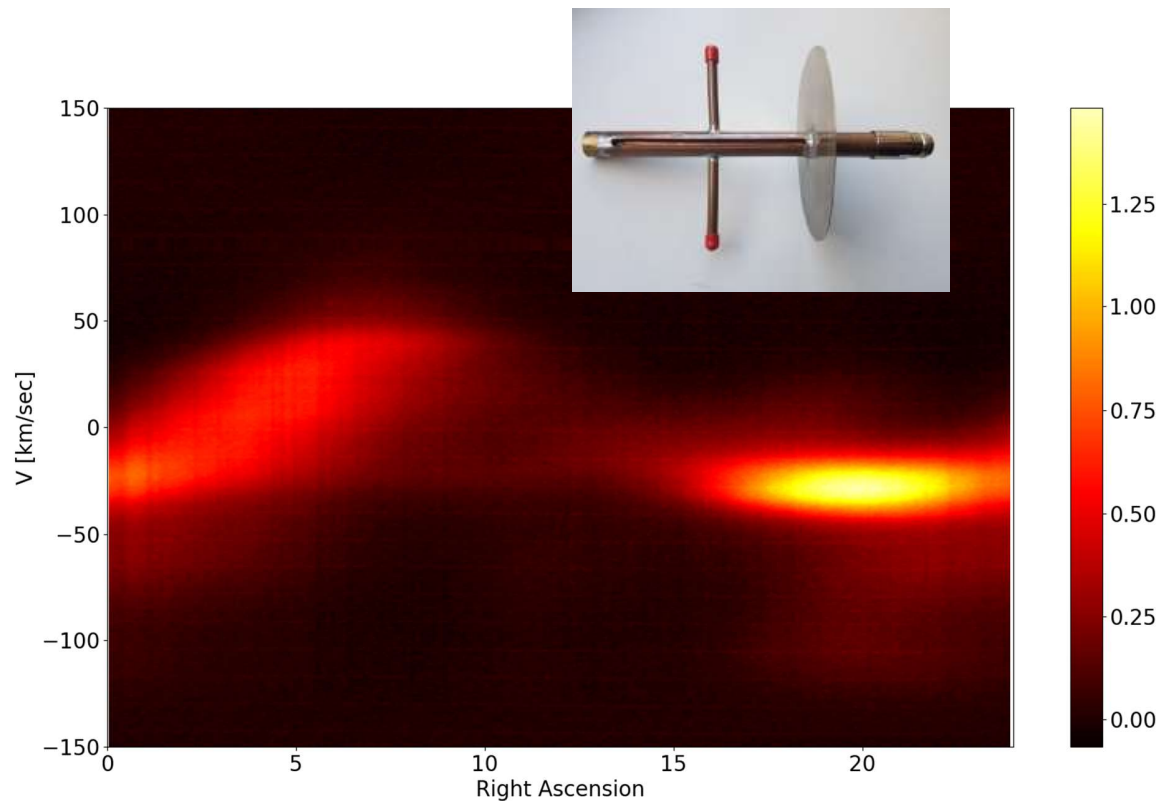


Figure 28: Transit scan with the dipole with reflector, variant

For this antenna, we have measured the best SNR of 95 at the RA position of 19:39. The spectrum at that position is shown in fig. 29.

We have also added a graph showing the spectra from the two dipoles with reflector in direct comparison (fig. 30).

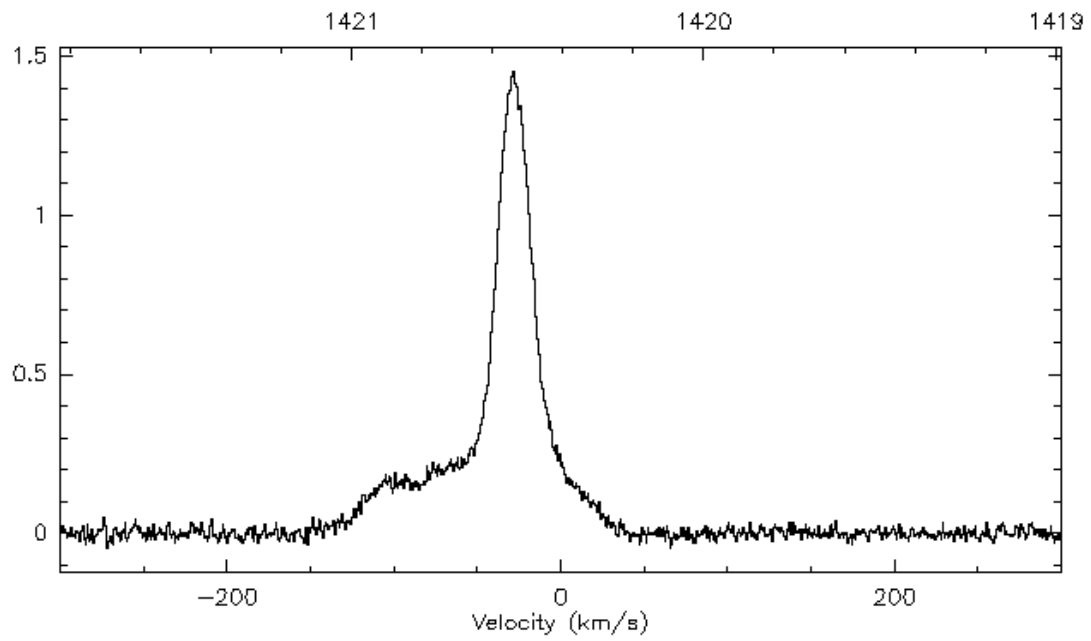


Figure 29: Spectrum with the dipole with reflector (variant)

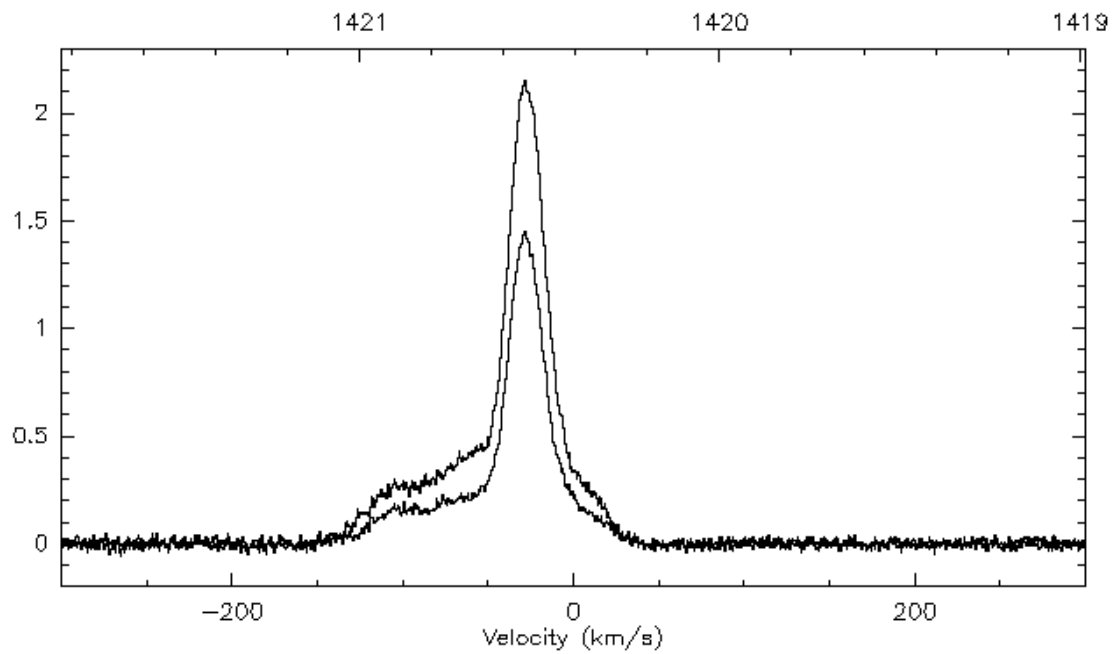


Figure 30: Direct comparison of the two dipoles with reflector
The lower curve is the variant

5.12. SETI Horn of Plenty

The SETI Horn of Plenty is a well-known design for an antenna at the 21 cm wavelength range and has successfully been used by many amateurs. Compared to the other antennas which we had tested, we were disappointed by the performance of our implementation of the SETI Horn. Given its fairly large aperture we had expected a better SNR.

We believe, however, that this is not due to the SETI Horn design itself, but due to our specific implementation. Using aluminium mesh to cover the structure we ended up with a fairly “wavy” surface. Also, the dimensions at the narrow end were different from the design due to some mechanical limitations. So, the results we achieved may not be representative. With a better implementation the performance of the SETI Horn would most likely be better.

The transit is shown in fig. 31. It can be noticed that even though the SNR is not as good as expected, the structure displayed in the transit scan is more detailed than for the smaller antennas. It is similar to the resolution of the corner cube antenna or the 60 cm dish. This indicates that the beam width is similar to these two antennas, as expected.

The best SNR of 81 was achieved at RA 21:17. The corresponding spectrum is shown in fig. 32.

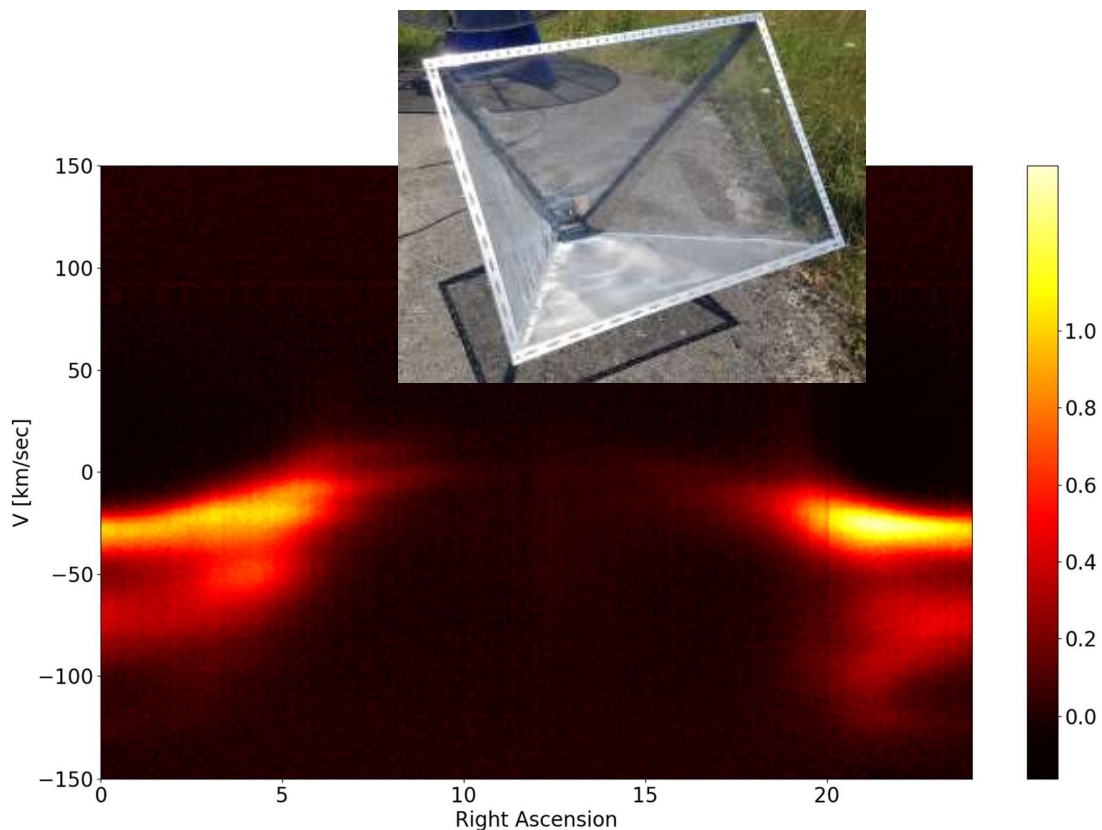


Figure 31: Transit scan with the SETI Horn of Plenty

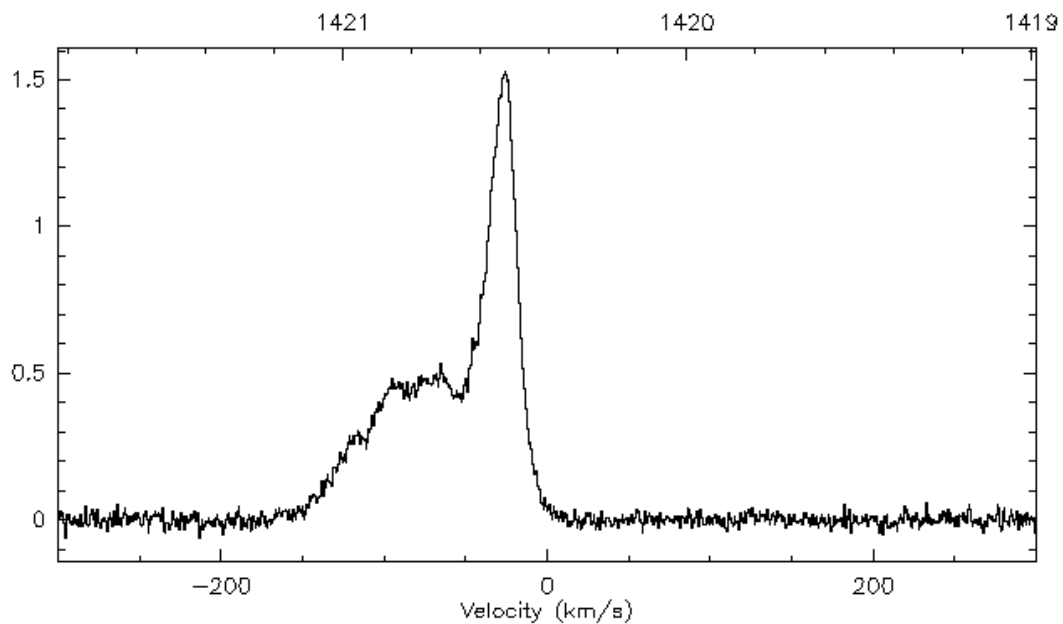


Figure 32: Spectrum with the SETI horn of Plenty at RA 21:17; SNR 81

5.13. “Crazy box”

We called this antenna “Crazy Box” because it seems such a strange idea to build a wooden box, cover it with aluminium foil and add a probe to make an antenna. Fundamentally it is a rectangular waveguide similar to the one in 5.9.

Despite the funny design this “antenna” works quite reasonably. The transit of the galactic plane can clearly be seen as shown in fig. 33.

The best signal to noise ratio is achieved at RA 19:51 with 79. The corresponding spectrum is shown in fig. 34.

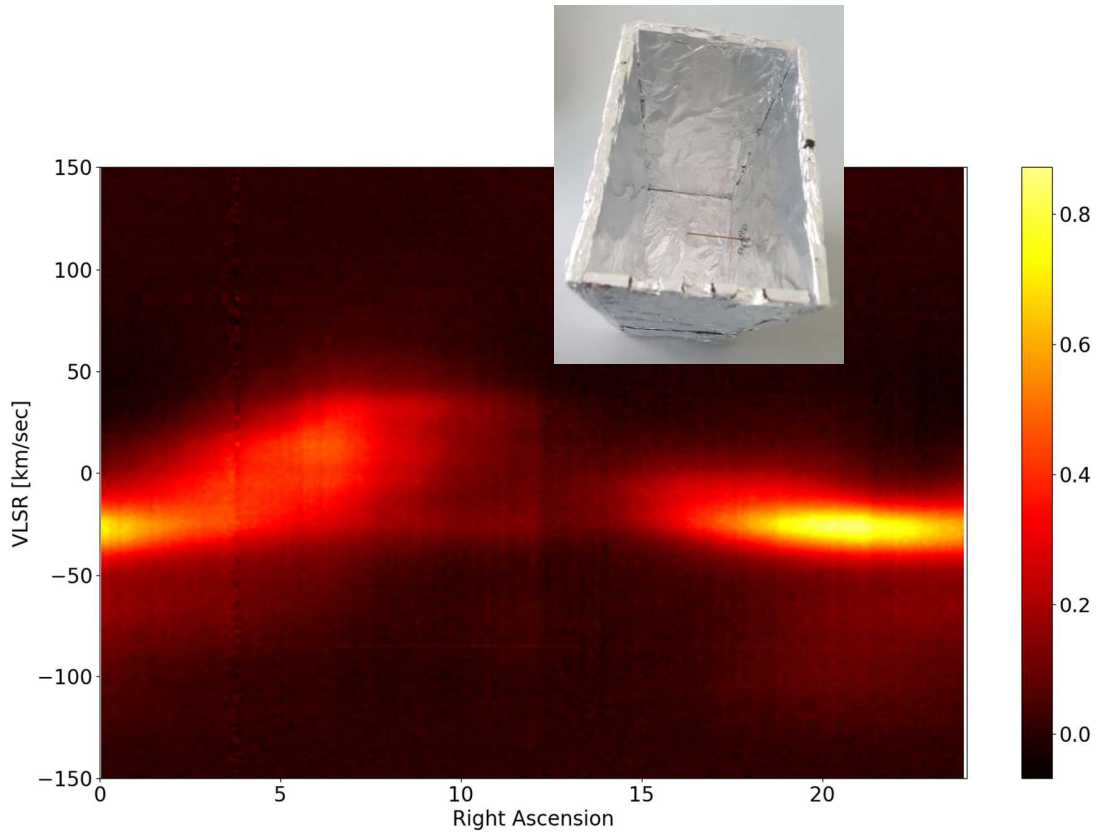


Figure 33: Transit scan with the "Crazy Box"

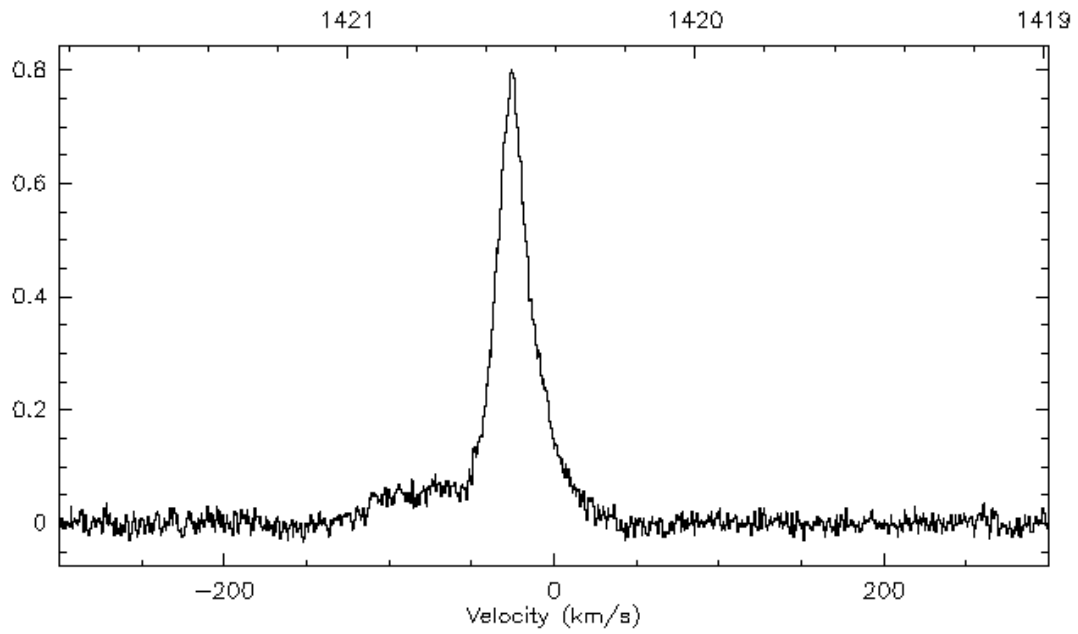


Figure 34: Spectrum with the "Crazy Box" antenna at RA 19:51; SNR 79

5.14. Simple half wave dipole

Can a simple dipole be used to detect the hydrogen emission?

The answer is a clear “yes” as can be seen in fig. 35. Even though spatial resolution is limited and the signal is a bit noisy, the dual transit of the galactic plane becomes clearly visible.

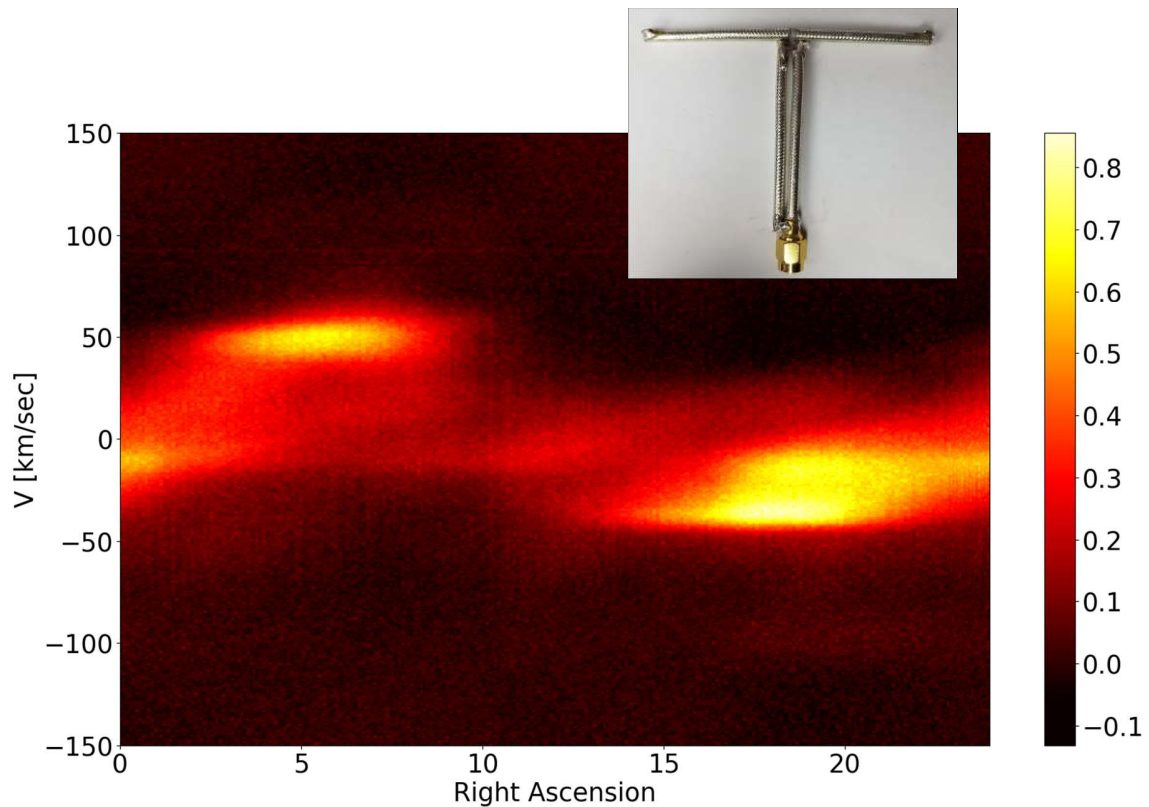


Figure 35: Transit scan with a simple dipole

The best signal to rms noise of 48 was achieved at RA 17:18, a bit different from the antennas before. The potential reason for this will be addressed in section 6 of this article.

The spectrum at that position is shown in fig. 36.

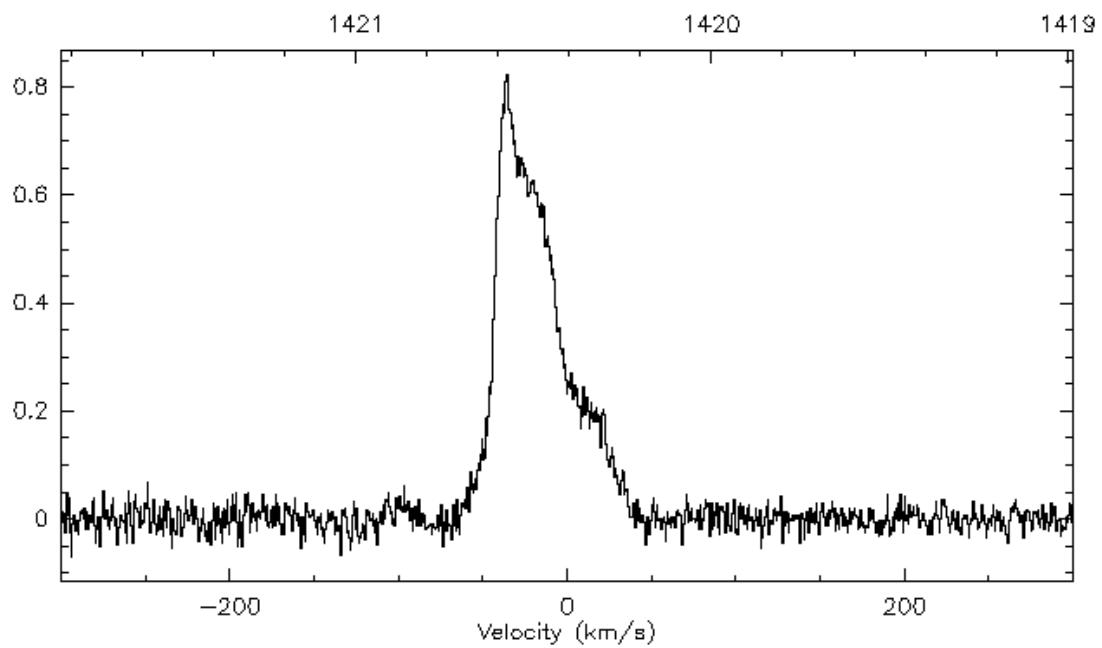


Figure 36: Spectrum with the dipole at RA 17:18; SNR 48

6. Summary and interpretation of results

The SNR achieved at respective the Best Spot (see 4.1 for definition) during the transit for each antenna is listed in table 1. The Best Spot is given in both RA/Dec and galactic coordinates.

Antenna	SNR at Best Spot	Right ascension of Best Spot (Declination always 50.5°)	Galactic longitude/latitude of Best Spot
3 m Dish	528 (27.2 dB)	04:34	154° / 1.9°
90 cm Dish	260 (24.1 dB)	20:44	89° / 4.9°
Corner Cube	231 (23.6 dB)	21:30	94° / -0.5°
60 cm Dish	212 (23.3 dB)	19:54	84° / 11.5°
L-Band Horn	198 (23.0 dB)	22:06	98° / -4.2°
Patch Yagi	167 (22.2 dB)	03:04	143° / -7.0°
“Stove Pipe”	135 (21.3 dB)	19:36	83° / 14.0°
Dipole with Reflector	121 (20.8 dB)	19:38	83° / 15.4°
L-Band Adapter	111 (20.5 dB)	20:34	88° / 6.1°
Patch Antenna	100 (20.0 dB)	20:10	85° / 9.3°
Dipole w. Reflector #2	95 (19.8 dB)	19:39	83° / 13.5°
Seti Horn of Plenty	81 (19.1 dB)	21:17	92° / 0.9°
“Crazy Box”	79 (19.0 dB)	19:51	84° / 11.9°
Dipole	48 (16.8 dB)	17:18	77° / 35°

Table 1: Summary of SNR at Best Spot

In section 8 of the first part of this series of articles [6] we have explained that a small antenna with low gain will benefit from its wide opening angle when observing an extended source like the hydrogen clouds. Therefore, while a small antenna has a smaller effective receiving area this is partially compensated as a larger volume of hydrogen in the sky is observed. This is confirmed by the results shown above. As an example, one can compare the 3 m dish with the dipole: The theoretical difference in gain between the 3 m dish and the simple dipole is about 560 [6], but from table 1 we see that the difference in signal to rms noise is only a factor 11.

Of course, there is also a downside of the larger angle: The spatial resolution becomes poorer with the wider opening angle and thus less detail of the structure of the hydrogen clouds passing through the antenna beam is resolved. A good demonstration of this is the transit scan of the 3 m dish with an opening angle of 5° (fig. 8) and the 90 cm dish with an opening angle of about 17° (fig. 10). While the

same basic structure can be seen, the latter is much more blurred. Going to even wider opening angles, the structure becomes even less defined as can be seen from the heatmaps for the different smaller antennas.

However, even for a dipole antenna it can be seen that the galactic plane passes twice during a day.

In the plot below, fig. 37, the red dots show at which position the boresight of the antenna was pointing at the time when the best signal was received (the Best Spot). One would expect that this is the case with the boresight pointing near the galactic plane. This can be found more or less for the majority of the antennas. One has to consider, however, that antennas may not have a perfect circular beam pattern. Asymmetries will occur and therefore deviation will be observable. A specific exception in that respect is the simple dipole where the Best Spot deviates quite a bit from the galactic plane and is found at 35° latitude. This may have been caused by the setup: The antenna was directly connected to the LNA which is in a metallic housing. The short distance between the dipole and the metallic housing may have resulted in an asymmetry of the antenna pattern. Clarity can only be achieved by measuring the antenna pattern including this housing which was not done in the context of this project.

For fig. 37 please note that the size of the dots does not represent the beam widths of the antennas, these would be much larger. The dots merely indicate the boresight pointing position.

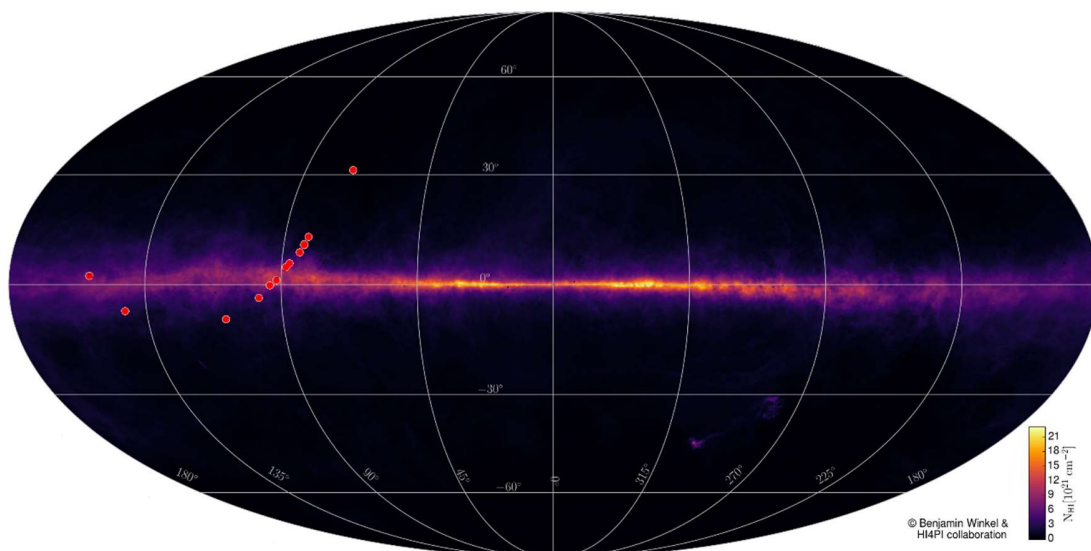


Figure 37: Location of the Best Spot for the antennas (red dots)
Source of Background Picture: Benjamin Winkel and the HI4PI Collaboration [1]

7. Conclusions

There is one overarching conclusion: When it comes to antennas for hydrogen observations, anything goes! Even the smallest and simplest antennas provide a discernible signal from the hydrogen emission of the galactic plane. Such experiments, where the reception of hydrogen emission using simple setups has been demonstrated, are also known from Michiel Klaassen [7] and Jan Lustrup [8].

Looking at the various antennas there are some options which seem to be specifically easy to make, yet still deliver a nice signal and at least a little bit of spatial resolution. Our favourites in this respect are the “stove pipe” and the corner cube antenna. The material for these antennas can be bought cheaply from hardware stores and there is very little tooling required to make them.

Amateurs entering the field of observation of galactic hydrogen thus have a wide choice of antennas. They can start with a simple antenna which suits their mechanical skills to get first results. With increasing ambition, one can move up to bigger and more complex antennas.

8. References

- [1] <https://astro.uni-bonn.de/~bwinkel/research.html>
- [2] https://github.com/xmikos/soapy_power
- [3] <https://github.com/pothosware/SoapySDR/wiki>
- [4] <https://en.wikipedia.org/wiki/FITS>
- [5] <https://www.iram.fr/IRAMFR/GILDAS/>
- [6] W.Herrmann, SARA Journal November-December, 39 (2018)
- [7] <http://parac.eu/projectmk9.htm>
- [8] <https://groups.google.com/forum/#!topic/sara-list/4dHKoch9ZL0>